

CIAMTIS

U.S. DOT Region 3 University Transportation Center

Development of a Practical Risk Framework for Railway Bridge Stiffness Transitions

August 31, 2020

Prepared by:

Joseph W. Palese and Ahmed Lasisi
Department of Civil and Environmental Engineering
University of Delaware

r3utc.psu.edu



**LARSON
TRANSPORTATION
INSTITUTE**

1. Report No. CIAM-UTC-REG2		2. Government Accession No.		3. Recipient's Catalog No.	
4. Title and Subtitle Development of a Practical Risk Framework for Railway Bridge Stiffness Transitions				5. Report Date August 31, 2020	
				6. Performing Organization Code	
7. Author(s) Joseph W. Palese, MBA, PE; https://orcid.org/0000-0003-3946-3777 and Ahmed Lasisi				8. Performing Organization Report No.	
9. Performing Organization Name and Address Department of Civil and Environmental Engineering University of Delaware DuPont Hall, 127 The Green Newark, DE 19716				10. Work Unit No. (TRAIS)	
				11. Contract or Grant No. 69A3551847103	
12. Sponsoring Agency Name and Address U.S. Department of Transportation Research and Innovative Technology Administration 3rd Fl, East Bldg E33-461 1200 New Jersey Ave, SE Washington, DC 20590				13. Type of Report and Period Covered Final Report 01/19/2019 – 08/31/2020	
				14. Sponsoring Agency Code	
15. Supplementary Notes Work funded through The Pennsylvania State University through the University Transportation Center Grant Agreement, Grant No. 69A3551847103.					
16. Abstract The objective of this research was to take advantage of historic measurement cycles to develop a risk index for bridge transitions that takes into account the stiffness differential (mean stiffness between zones), stiffness variation (variation around the mean), train axle load, train operating speed, rate of degradation of the transition zone, length of the bridge, and other factors. The data utilized to achieve this objective were vertical track deflection data and railway operating data for approximately 500 miles of railway with nearly 100 bridges. This research activity resulted in a framework for practically implementing a risk index for bridge transitions that allows the railway to prioritize bridges for maintenance and/or remedial action as well as monitor the health of bridge transitions. In addition, the resulting framework has the ability to identify the most cost-effective approach to managing the bridge transitions, status quo maintenance, implementation of a transition zone (and best approach), or matching stiffness through the bridge. Since the data utilized were very well known to the railway, and the resulting outcome is an easy-to-use and practical framework, it is expected that acceptance by industry partners will be timely and well received.					
17. Key Words Bridge transitions, risk index, train axle load, operating speed, vertical track deflection, stiffness differential, degradation				18. Distribution Statement No restrictions. This document is available from the National Technical Information Service, Springfield, VA 22161	
19. Security Classif. (of this report) Unclassified		20. Security Classif. (of this page) Unclassified		21. No. of Pages 75	22. Price

DISCLAIMER

The contents of this report reflect the views of the authors, who are responsible for the facts and the accuracy of the information presented herein. This document is disseminated in the interest of information exchange. The report is funded, partially or entirely, by a grant from the U.S. Department of Transportation's University Transportation Centers Program. However, the U.S. Government assumes no liability for the contents or use thereof.

TABLE OF CONTENTS

List of Figures	iv
List of Tables	v
1. Introduction	1
2. Analytic Methods	4
Beam on Elastic Foundation	4
Dynamic Force Simulation	8
3. Data Collection and Management	15
Data Collection	17
Exploratory Data Analysis	17
Data Preparation.....	21
4. Development of Risk Framework	26
Dynamic Simulation	26
Speed Effect	28
Identification of Stiffness Transition Zones	30
Transition Risk Model	31
5. Application of Risk Framework	34
6. Concluding Remarks	38
Summary of Research	38
Future Research	39
References	40

LIST OF FIGURES

Figure 1. Stiffness transition model.....	1
Figure 2. MRail measurement at a bridge transition.....	2
Figure 3. Beam on elastic foundation for single wheel load.....	4
Figure 4. Sample BOEF solution for one wheel for deflection basin.....	6
Figure 5. Deflection map for single wheel load.....	6
Figure 6. Deflection map for step change in stiffness.....	8
Figure 7. Eighth-car model on a ramp.....	9
Figure 8. EFCM physical model.....	11
Figure 9. ECFM developed in Simulink.....	12
Figure 10. Vertical velocity excitation for input.....	13
Figure 11. Dynamic force output along deflection map.....	13
Figure 12. Mrail vertical track deflection measurement system.....	15
Figure 13. MRail Yrel measurement defined.....	16
Figure 14. Sample MRail output report.....	16
Figure 15. Track sections for data acquisition and analysis.....	17
Figure 16. Density distributions for the three study routes.....	18
Figure 17. Right rail Yrel distribution comparison.....	19
Figure 18. Typical Yrel output for 5 miles of track.....	20
Figure 19. Stiffness variation visible in Yrel (507.0 – 507.5).....	21
Figure 20. FFT of Yrel data for 507.0 – 507.5.....	21
Figure 21. EMD of Yrel.....	23
Figure 22. Original and smoothed Yrel.....	25
Figure 23. Vertical velocity profile for MP 507.0 to 507.5.....	27
Figure 24. Simulink vertical dynamic force output.....	27
Figure 25. Velocity excitation for BOEF step change in stiffness for various speeds.....	28
Figure 26. Simulated dynamic force output for various speeds.....	29
Figure 27. Summary plot of speed sensitivity results.....	30
Figure 28. Defined transition zones.....	31
Figure 29. Comparison of Simulink and slope method.....	32
Figure 30. Transition Zone comparison of Simulink and slope method.....	32
Figure 31. Sensitivity analysis of risk model.....	33
Figure 32. Example application of risk framework.....	34
Figure 33. Max risk distribution for each study segment.....	36

LIST OF TABLES

Table 1. Dyanmic load using maximum slope approach.....	10
Table 2. Track segments and inspection dates.....	17
Table 3. Yrel summary statistics for the three segments.	19
Table 4. Summary output for speed sensitivity.	29
Table 5. Summary statistics of risk values for each study.....	35
Table 6. Example risk thresholds.....	37
Table 7. Application of thresholds summary.....	37

1. Introduction

Railway bridges often suffer accelerated degradation at bridge approaches due to an abrupt change in vertical track stiffness. As a train travels from ballasted track onto a bridge, the sudden change in vertical track support stiffness (from softer track to stiffer track) results in dynamic impact forces that causes a degradation of track geometry resulting in poor ride quality and damage to track components, vehicle/lading components, and bridge components. As the geometry at this location degrades, the impact forces are exacerbated, resulting in an accelerated rate of geometry degradation and differential settlement. This results in accelerated rates of component failure as well as a significant increase in track maintenance (surfacing of the track). This cost has been estimated at well over \$200M annually for U.S. railways (Stark, Wilk, & Rose, 2016).

Understanding the mechanics of this problem has been the focus of much research (Kerr, 2003). The track can be modeled as a beam on elastic foundation with the transition modeled as a step function change in stiffness. The governing equation and model are shown in Figure 1 (Zarembski, Palese, & Katz, 1999). Numerous researchers have focused their attention on the levels of impact forces for various stiffness differentials and resulting damage.

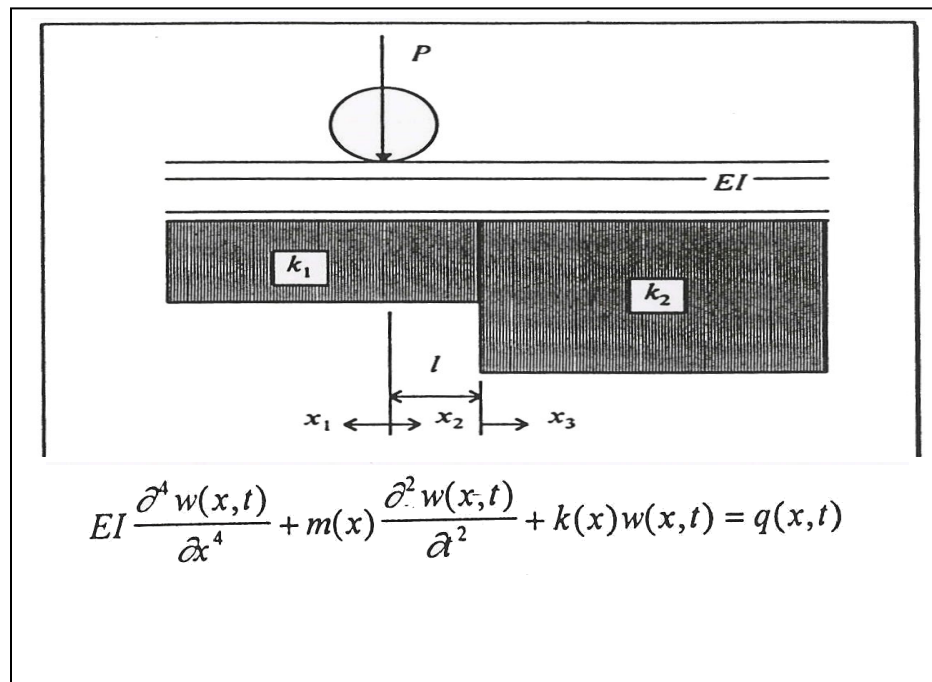


Figure 1. Stiffness transition model

There has also been much research on methods for alleviating these impact forces. There are two primary approaches in practice today: (1) introducing a transition from the soft stiffness of the parent track to the stiffer value inherent on the bridge, and (2) matching the parent track stiffness by softening the stiffness on the bridge. Method 1 utilizes transition zones (of defined length based on stiffness differential, load, and operating speed). These transition zones can be accomplished by using different tie sizes, elastomeric rail pads or ballast mats to gradually change stiffness, transition slabs made of concrete or asphalt (between the subgrade and ballast) to gradually change stiffness, and others (Li, Otter, & Carr, 2010). Method 2 aims to match the stiffness on the bridge to that of the parent track by using elastomeric rail or ballast (under-tie) pads such that there is no stiffness transition (Kerr & Moroney, 1993). For all of the aforementioned remedial actions, it is important to know the stiffness differential as well as the load operating environments and speeds.

A recently introduced autonomous inspection system (MRail) measures the vertical track deflection along the track and provides the necessary data on track stiffness (Farritor, 2013) that can be used in the development of these remedial actions. In addition, as these data are collected frequently, the ability to analyze the rate of degradation of the transition area exists. Figure 2 shows typical vertical track deflection measurements in the area of a bridge transition. Note the mean stiffness differential between zones as well as the variation around the mean (i.e., the stiffness is not uniform).

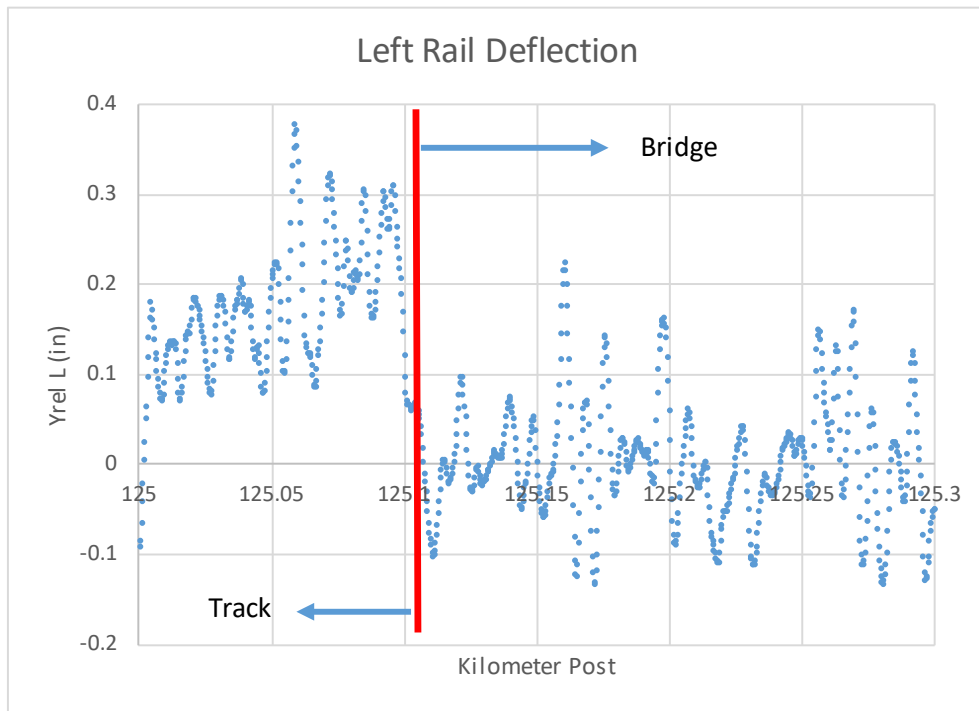


Figure 2. MRail measurement at a bridge transition

The objective of this research was to take advantage of historic measurement cycles to develop a risk index for bridge transitions that takes into account the stiffness differential (mean stiffness between zones), stiffness variation (variation around the mean), train axle load, train operating speed, rate of degradation of the transition zone, length of the bridge, and other factors. The data utilized to achieve this objective were vertical track deflection data and railway operating data that were gathered over several runs in the course of one year. These data were readily available to the research team for approximately 500 miles of railway, with nearly a hundred bridges.

This research activity resulted in a framework for practically implementing a risk index for bridge transitions that allows the railway to prioritize bridges for maintenance and/or remedial action as well as monitor the health of bridge transitions. In addition, the resulting framework has the ability to identify the most cost-effective approach to managing the bridge transitions, status quo maintenance, implementation of a transition zone (and best approach), or matching stiffness through the bridge. Since the data utilized were very well known to the railway, and the resulting outcome is an easy-to-use and practical framework, it is expected that acceptance by industry partners will be timely and well received.

2. Analytic Methods

Beam on elastic foundation theory is often utilized to quantify and understand stresses in the railroad track structure. This approach utilizes the track stiffness as a direct input, and the resulting stresses in the track components (rail, fastener, ties, ballast, and subgrade) are a function of the load, track stiffness, and component material and geometric properties.

In addition, dynamic simulation modeling is utilized to understand the dynamic force environment associated with passing trains as a function of speed, mass, and dynamic properties of the vehicle and track. Sophisticated dynamic simulation models exist, as well as simplified modeling approaches to understand this load environment.

Background to these approaches follows, in the context of application to risk analysis of stiffness transitions.

BEAM ON ELASTIC FOUNDATION

Traditional beam on elastic foundation (BOEF) analysis assumes a uniform stiffness supporting the rail. The track stiffness, or track modulus, is comprised of the stiffness elements combined for all the supporting components of the rail (tie/fastener, ballast and subgrade), with the subgrade being the largest contributor to the uniform track stiffness. The stiffness is generally assumed to be linear, though bilinear and nonlinear track stiffness have been modeled. For a single wheel, the rail behaves as an infinite beam on a uniform elastic foundation, as shown in Figure 3.

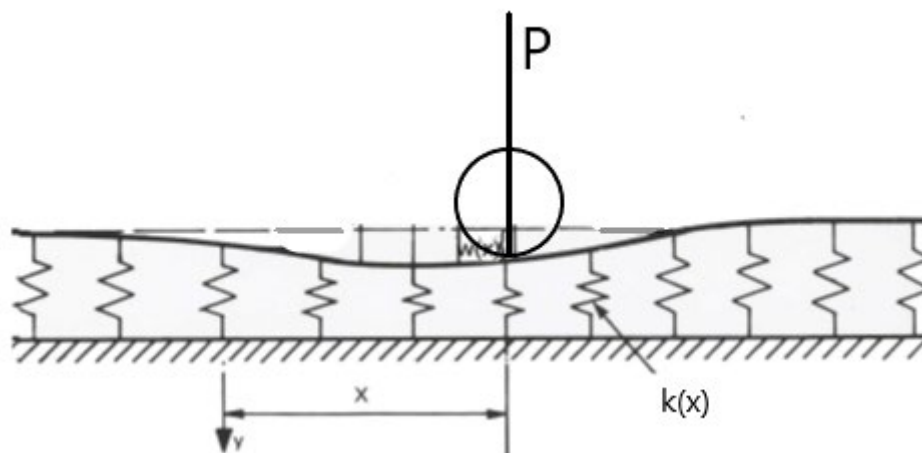


Figure 3. Beam on elastic foundation for single wheel load

The formulation and solution of this classic problem can be found in many sources (Hetenyi, 1946), and is summarized below¹.

$$EI \frac{d^4 w(x)}{dx^4} + kw(x) = 0$$

$$\lim_{x \rightarrow \infty} \left(w(x), \frac{dw(x)}{dx} \right) \rightarrow \text{finite}, \quad \frac{dw(0)}{dx} = 0, \quad \frac{d^3 w(0)}{dx^3} = \frac{P}{2EI}$$

$$w(x) = \frac{P\beta}{2k} e^{-\beta|x|} [\cos(\beta|x|) + \sin(\beta|x|)]$$

Where

$w(x)$ = rail deflection at location x

P = wheel load

k = track modulus or stiffness

E = rail modulus of elasticity

I = rail moment of inertia

$$\beta = \sqrt[4]{\frac{k}{4EI}}$$

This solution can also be applied for multiple wheels using linear superposition and summing solutions. Note that this solution is often utilized in a quasi-static implementation by augmenting the applied load for dynamic effects. A sample application of this solution is shown in Figure 4 for a 286,000-lb car traveling at 60 mph for soft ($k = 3,000$ lb/in/in) and stiff ($k = 7,000$ lb/in/in) track, where the maximum deflection occurs under the wheel. This is referred to as the deflection basin, whereby the responding pressure of the track, integrated along the track's longitudinal axis, is equal to the applied load.

¹ Note the solution is for a fourth order homogenous differential equation, assuming symmetry.

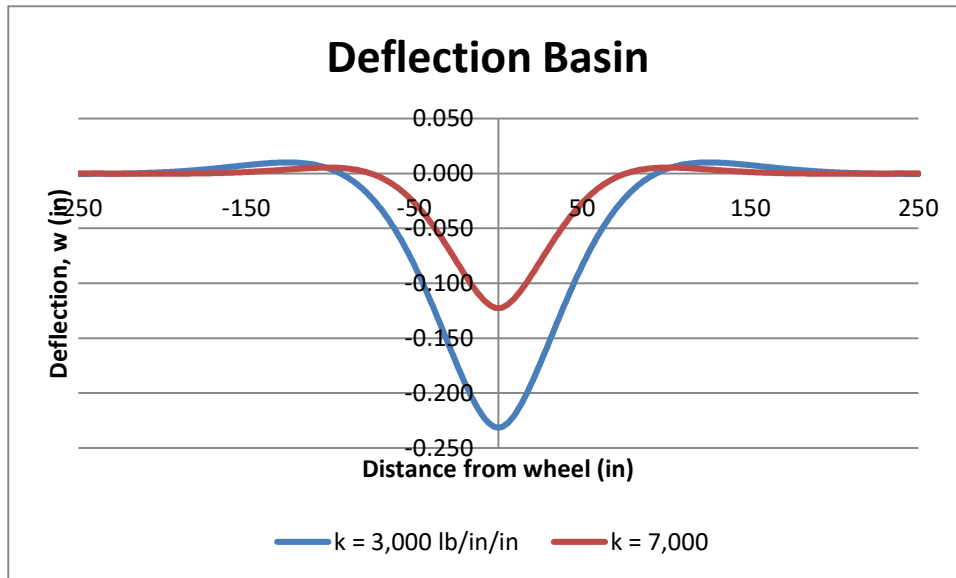


Figure 4. Sample BOEF solution for one wheel for deflection basin.

It is important to note that this model results in a uniform maximum deflection at every location of applied wheel load along the track's longitudinal axis, which is referred to as the deflection map. This is shown in Figure 5 for the same example shown previously in Figure 4.

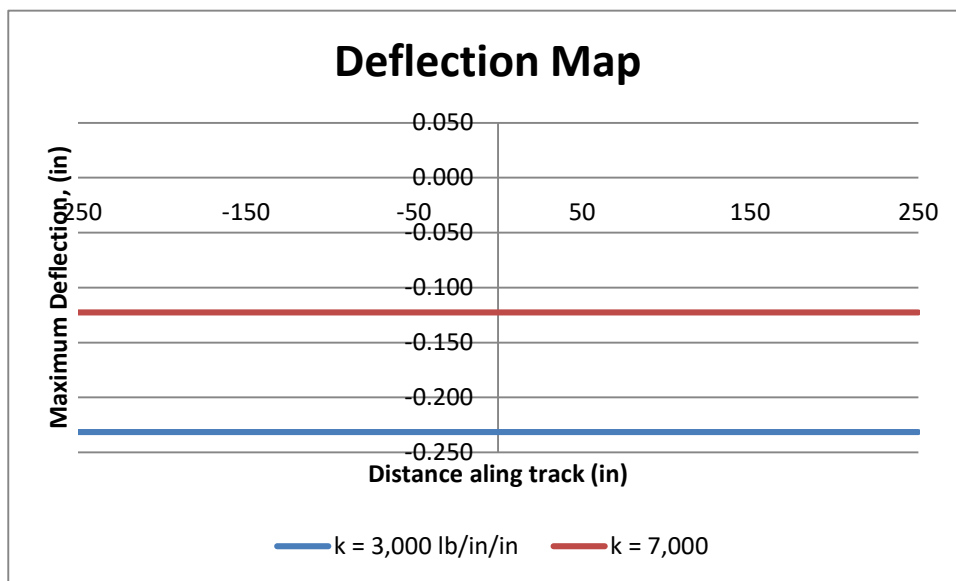


Figure 5. Deflection map for single wheel load.

Thus, the uniform maximum deflection for the same car traveling over stiff versus soft track is reduced nearly 50%.

When considering a track stiffness change, a step function in uniform stiffness can be modeled as previously shown in Figure 1. To determine the deflection at any given point along the track, the

formulation results in three differential equations with boundary and matching conditions. The formulation for this problem follows:

Differential Equations:

$$EI \frac{d^4 w_1(x_1)}{dx_1^4} + k_1 w_1(x_1) = 0 \quad -\infty < x_1 \leq 0$$

$$EI \frac{d^4 w_2(x_2)}{dx_2^4} + k_1 w_2(x_2) = 0 \quad 0 < x_2 \leq l$$

$$EI \frac{d^4 w_3(x_3)}{dx_3^4} + k_2 w_3(x_3) = 0 \quad 0 < x_3 \leq \infty$$

Boundary/Matching Conditions:

$$\lim_{x_1 \rightarrow -\infty} \left(w_1(x_1), \frac{dw_1(x_1)}{dx_1} \right) \rightarrow \text{finite}$$

$$\begin{aligned} w_1(0) &= w_2(0) \\ \frac{dw_1(0)}{dx_1} &= \frac{dw_2(0)}{dx_2} \\ \frac{d^2 w_1(0)}{dx_1^2} &= \frac{d^2 w_2(0)}{dx_2^2} \\ \frac{d^3 w_1(0)}{dx_1^3} - \frac{d^3 w_2(0)}{dx_2^3} &= -\frac{P}{EI} \end{aligned}$$

$$\begin{aligned} w_2(l) &= w_3(0) \\ \frac{dw_2(l)}{dx_2} &= \frac{dw_3(0)}{dx_3} \\ \frac{d^2 w_2(l)}{dx_2^2} &= \frac{d^2 w_3(0)}{dx_3^2} \\ \frac{d^3 w_2(l)}{dx_2^3} &= \frac{d^3 w_3(0)}{dx_3^3} \end{aligned} \quad \lim_{x_3 \rightarrow \infty} \left(w_3(x_3), \frac{dw_3(x_3)}{dx_3} \right) \rightarrow \text{finite}$$

The general form of the solution for this problem is:

$$w_i(x_i) = e^{-\beta_{n(i)} x_i} [A_{1i} \cos(\beta_{n(i)} x_i) + A_{2i} \sin(\beta_{n(i)} x_i)] + e^{\beta_{n(i)} x_i} [A_{3i} \cos(\beta_{n(i)} x_i) + A_{4i} \sin(\beta_{n(i)} x_i)]$$

Where

$w_i(x_i)$ = deflection for zone i

$i = 1$ to 3

$n(i) = 1, 1, 2$

$$\beta_{n(i)} = \sqrt[4]{\frac{k_{n(i)}}{4EI}}$$

A_{ji} = integration constants, ($j = 2$ to 4 , $i = 1$ to 3)

Applying the boundary/matching conditions results in the closed form solution for the 12 integration constants (Zaremski et al., 1999). Implementing this solution, the deflection map for the same vehicle transitioning between soft and stiff track is shown in Figure 6.

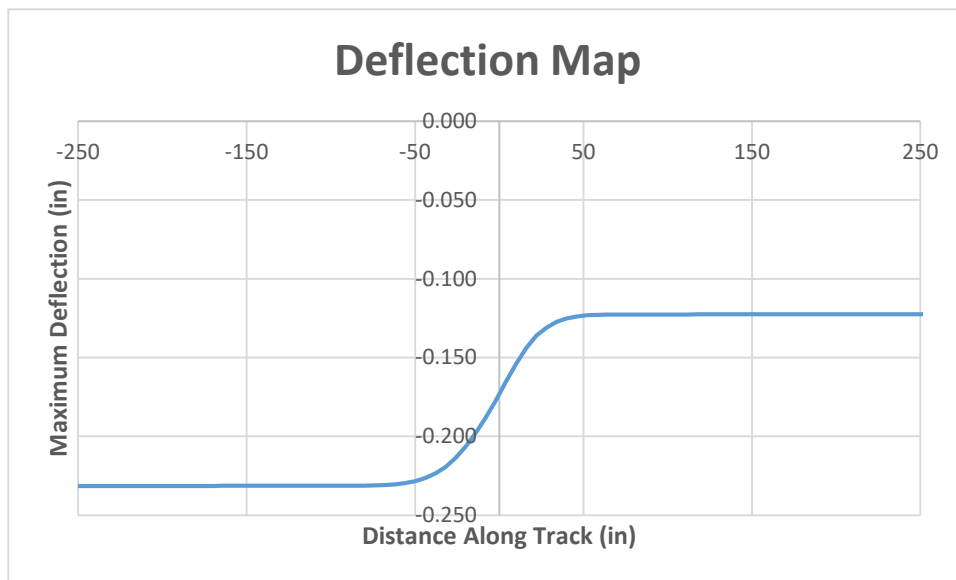


Figure 6. Deflection map for step change in stiffness.

It can be seen from Figure 6 that as a vehicle travels over an abrupt change in stiffness, a “ramp” will be experienced by the vehicle, whose length is a function of the bending stiffness of the rail, and the elevation difference is a function of the soft and stiff track modulus values. Note that the constant portions of the deflection map are identical to those in Figure 5 when away from the influence zone of the stiffness change. This “ramped” deflection map will result in vertical dynamic forces on the track by the passing vehicle.

DYNAMIC FORCE SIMULATION

While many sophisticated dynamic simulation models exist for track/train interaction, they are time consuming to implement and do not lend themselves to large-scale application. A simplified

quasi-static approach is to statically determine the vehicle's path, then apply a dynamic approach to this path. This method considers one wheel (with no mass) connected to an eighth of the car body mass via a spring/damper connection. This is shown in Figure 7 (for zero damping), along with the free-body diagram, whereby the deflection map (or path) from Figure 6 is simplified to be linear with abrupt changes (Palese, Zarembski, & Katz, 1998).

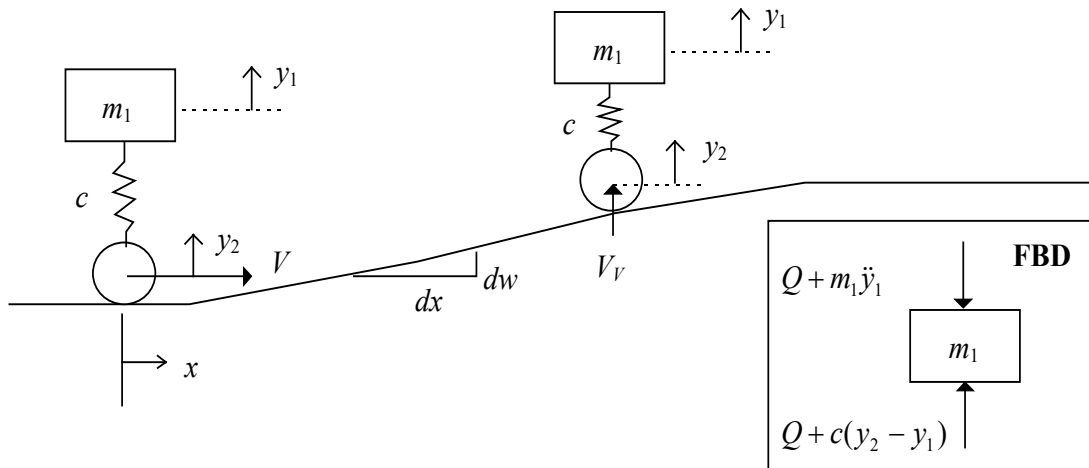


Figure 7. Eighth-car model on a ramp.

It can be seen from this model that as the wheel moves up (or down) the inclined portion of the path, dynamic action occurs, resulting in dynamic forces. Noting the free-body diagram (FBD) and summing the forces results in the following:

$$Q + c(y_2 - y_1) - Q - m_1\ddot{y}_1 = 0$$

Simplifying the above equation and noting that $y_2 = V_V t$ yields the governing differential equation as follows:

$$\ddot{y}_1 + \frac{c}{m_1} y_1 = \frac{cV_V}{m_1} t$$

with boundary conditions:

$$y(0) = 0$$

$$\dot{y}(0) = 0$$

The resulting solution for motion (noting the boundary conditions) is given as:

$$y(t) = V_V \left[-\frac{1}{\omega} \sin(\omega t) + t \right]$$

The vertical velocity component can be determined by the inclination and the velocity vector as follows:

$$V_V = V \frac{dw}{dx}$$

Where

V = the velocity of the vehicle

$\frac{dw}{dx}$ = the slope of the path of travel

Noting this, and that the dynamic force can be determined from the mass multiplied by the acceleration, the calculation for dynamic force becomes:

$$P_D = P_{ST} + m_1 \ddot{x}_{\max} = P_{ST} + V \sqrt{cm_1} \frac{dw}{dx}$$

The above solution is a simplified representation of the dynamic force and is conservative, as it does not consider any damping, lumps stiffness elements together, and only considers the abrupt slope change of the wheel's path.

For the 286,000-lb car previously analyzed, the results of applying this approach are shown in Table 1.

Table 1. Dyanmic load using maximum slope approach.

Car Weight	286,000 lb
Speed (V)	60 mph
Suspension (c)	40,000 lb/in
Dw/dx	0.00175 in/in
Pst	35,750 lb
Pd	39,311 lb
dP	3,561 lb

This simplified example results in a 10% additional dynamic force when traversing the abrupt stiffness change. It is important to note that the dynamic load effect changes linearly with vehicle speed, slope of track contour, and root of vehicle mass.

A more sophisticated method for determining the dynamic impact force is to construct a single-wheel dynamic simulation model that considers several masses and spring/damper connections (See Figure 8). Note that this is still less sophisticated than a full dynamic simulation model approach, which is time and computationally intensive. Such a single-wheel model, herein referred to as a one-eighth freight car model (EFCM), can be constructed using Matlab/Simulink (The Mathworks, 2019). Simulink provides an intuitive, object-based interface for building up a multi-degree-of-freedom simulation model.

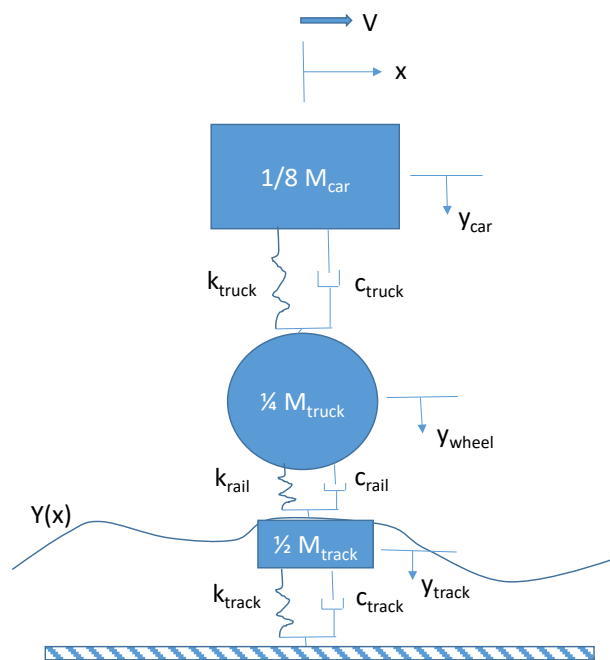


Figure 8. EFCM physical model.

An EFCM was developed in Simulink (see Figure 8 for a block diagram) that included the following critical elements:

- One-eighth car body sprung mass
 - Truck suspension stiffness
 - Truck linear damping
- One-fourth truck unsprung mass (wheel, half axle, half bolster, half side frame)
 - Wheel/rail Hertzian stiffness
 - Wheel/rail damping (assumed zero)
- One-half track mass (one rail, half tie)
 - Track stiffness
 - Track damping

The model accepts a velocity excitation between the track mass and the unsprung mass as input, which is developed in the time domain from the deflection map and vehicle speed (numeric differentiation). Thus for the 286,000-lb car previously modeled, traveling at 60 mph, given the deflection map from Figure 6, the vertical velocity excitation to the model shown in Figure 9 results.

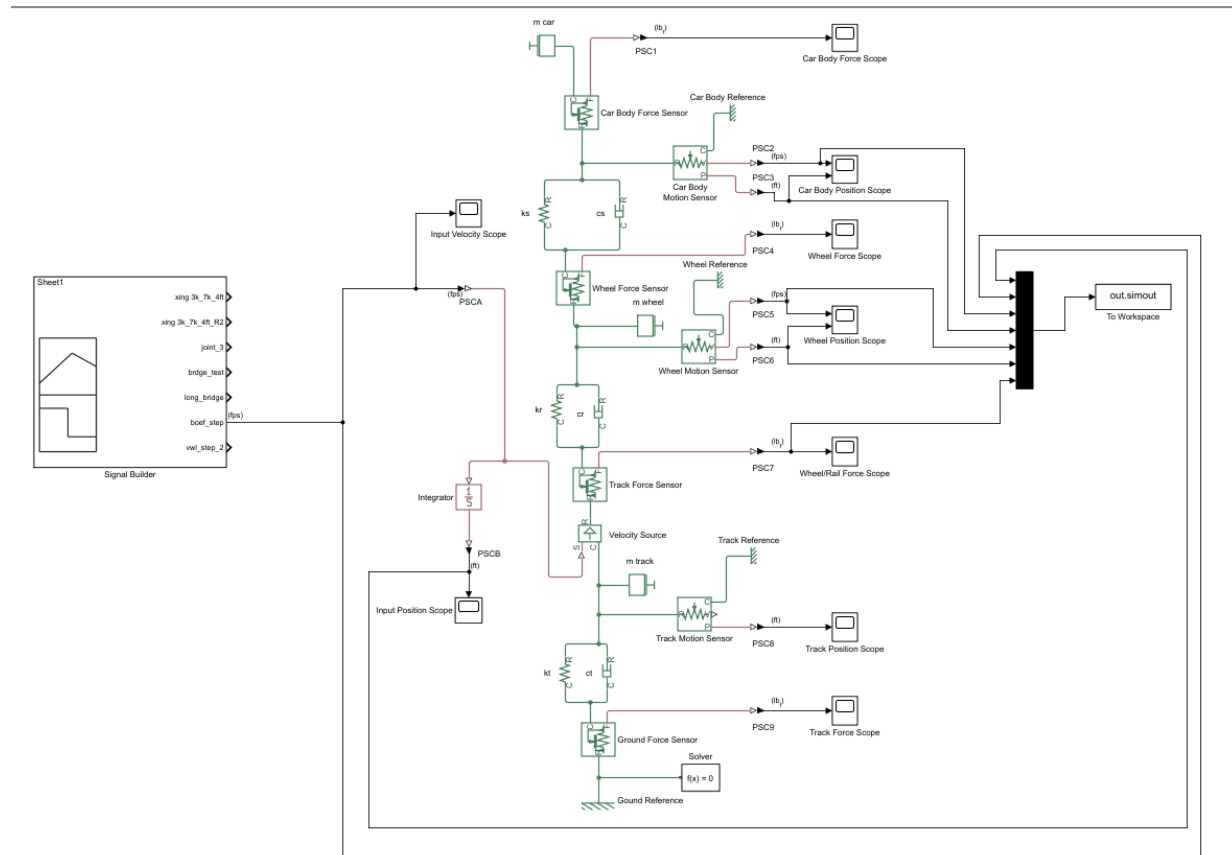


Figure 9. ECFM developed in Simulink.

While the model outputs velocity and displacement of the various masses with respect to various reference frames, the primary output of interest is the force on the wheel (between the unsprung mass and the sprung mass). This output force is shown in the time domain in Figure 10. Note that this is the dynamic component due to the input velocity excitation and is added to the downward gravitational force (weight) to obtain the total force value. The dynamic force output is shown in Figure 11.

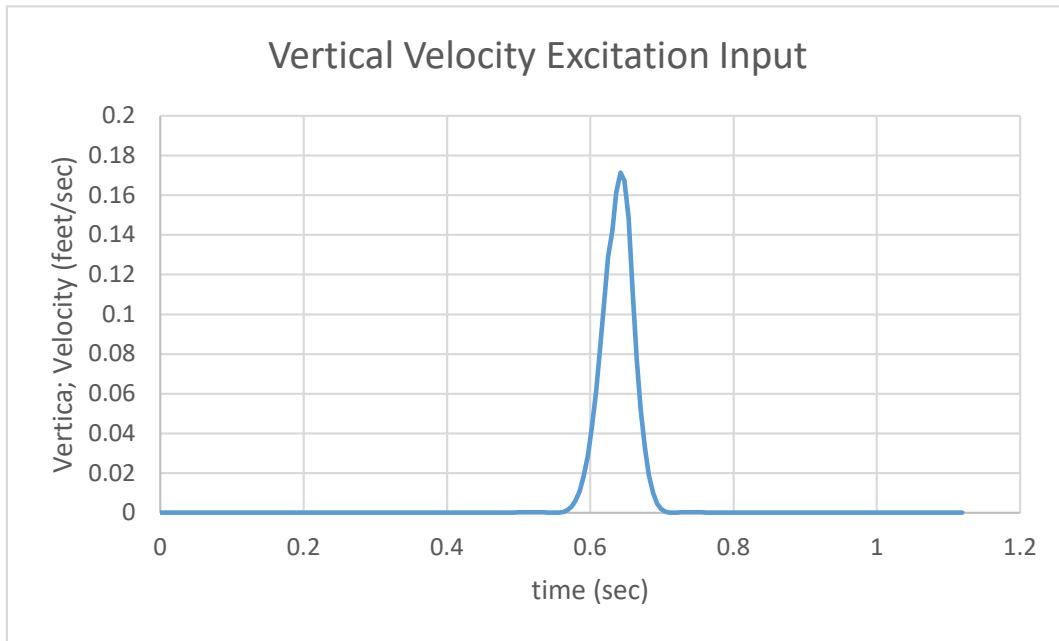


Figure 10. Vertical velocity excitation input.

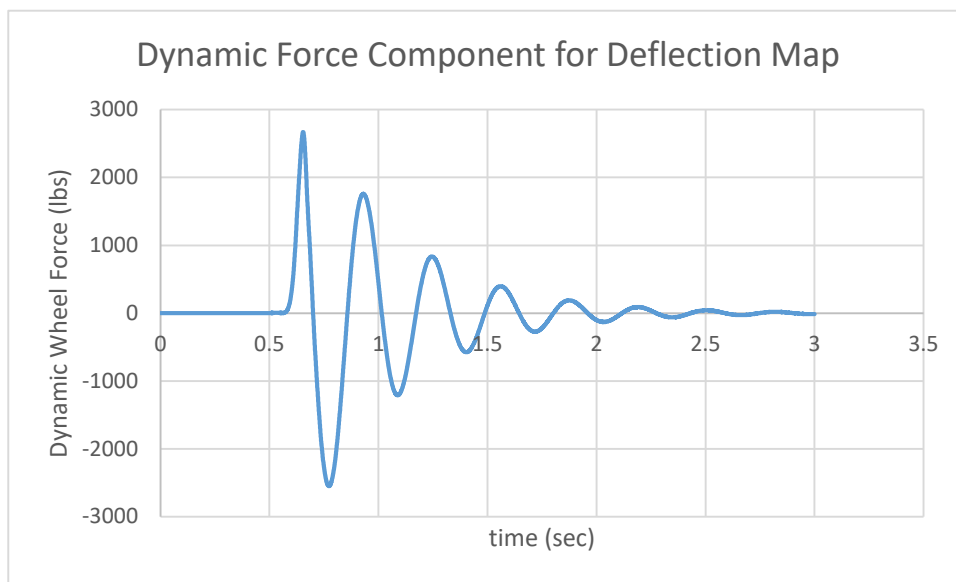


Figure 11. Dynamic force output along deflection map.

Thus, for this scenario, an increase in vertical force is a maximum of 2,550 lb (7% increase above the static wheel load), as induced by the vertical velocity excitation associated with the step change in deflection path (referred to as deflection map). This value is slightly less than the 3,561 lb (10% increase above the static wheel load) determined by the conservative analysis presented previously.

The primary value of this approach to determining dynamic forces is that a generic velocity profile can be input, as opposed to an impulse excitation velocity, which is a limitation of the simplistic

approach presented previously. In addition, time duration of forces associated with damping can be observed, as well as the effects of various mass/spring/damper components, such as unsprung mass of the wheel, mass of the track, etc.

This is the approach that was utilized with the vertical track deflection measurements to develop velocity input profiles to the wheel.

3. Data Collection and Management

The primary focus of this study was to evaluate data that were continuously collected with respect to track stiffness. Specifically, relative track stiffness is determined using the MRail vertical track deflection measurement system, which uses a laser/camera sensor system mounted to a three-piece truck (see Figure 12).

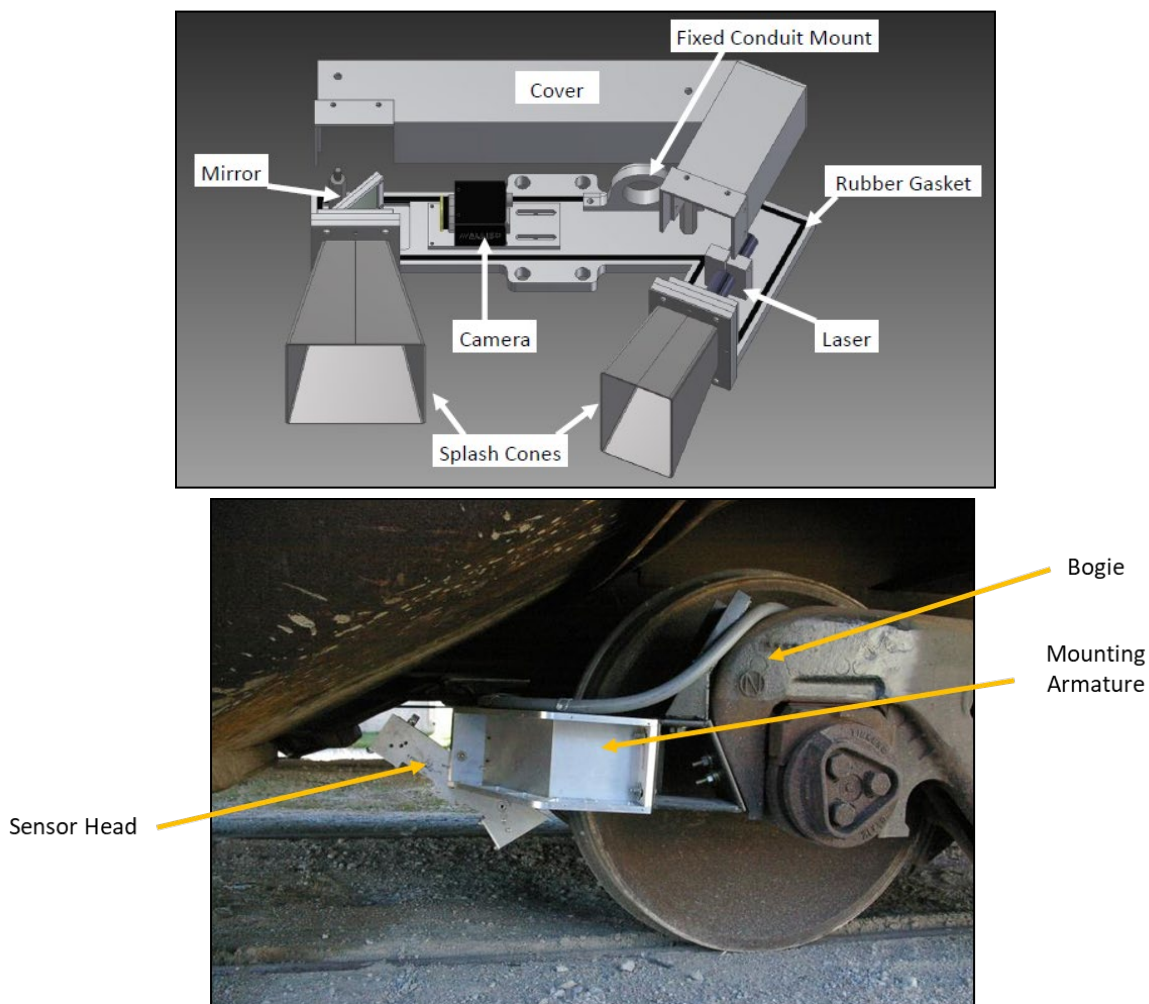


Figure 12. Mrail vertical track deflection measurement system.

This system measures a relative deflection (Y_{rel}) of the rail as defined in Figure 13 (Newman, 2014) approximately every foot of vehicle travel and stores these data for both the left and right rails. A sample output report of the system is shown in Figure 14, which contains Y_{rel} , a running roughness and heat map for each rail, along with summary statistics for a mile of track. These data are also stored electronically in ASCII format for further interrogation and analysis.

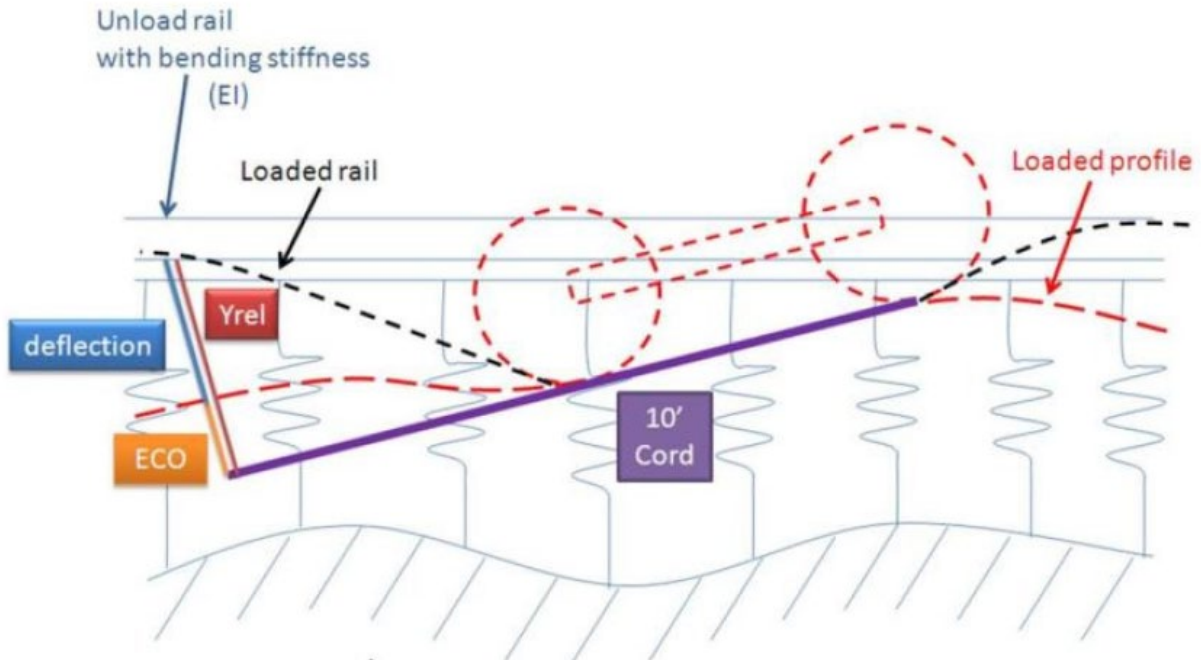


Figure 13. M-Rail Yrel measurement defined.

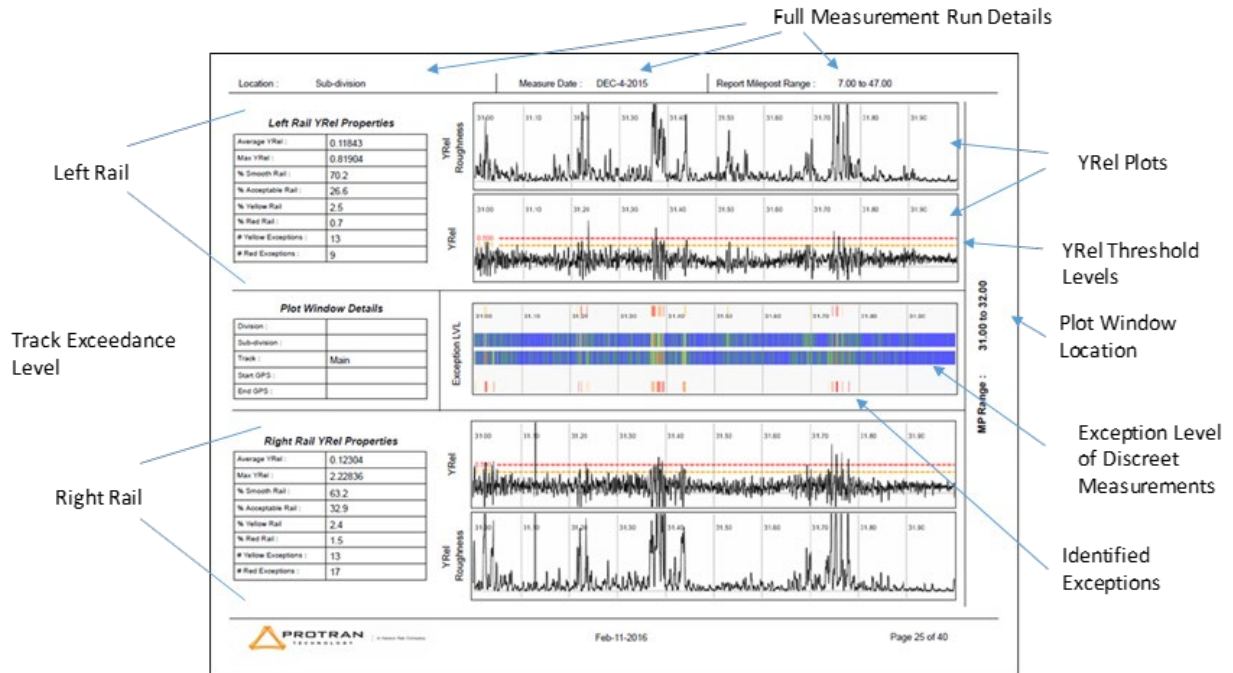


Figure 14. Sample M-Rail output report.

DATA COLLECTION

Data were obtained for a significant length of track (450 miles) that contained a number of bridges. These data were collected for several cycles over the course of one year. The railroad layout and specific track sections of interest for this study are shown in Figure 15. The left portion of the map (northern routes) shows section 1-8, and the left portion (southern routes) shows sections A-B and B-C. The segment specifics and dates of data collection are shown in Table 2.

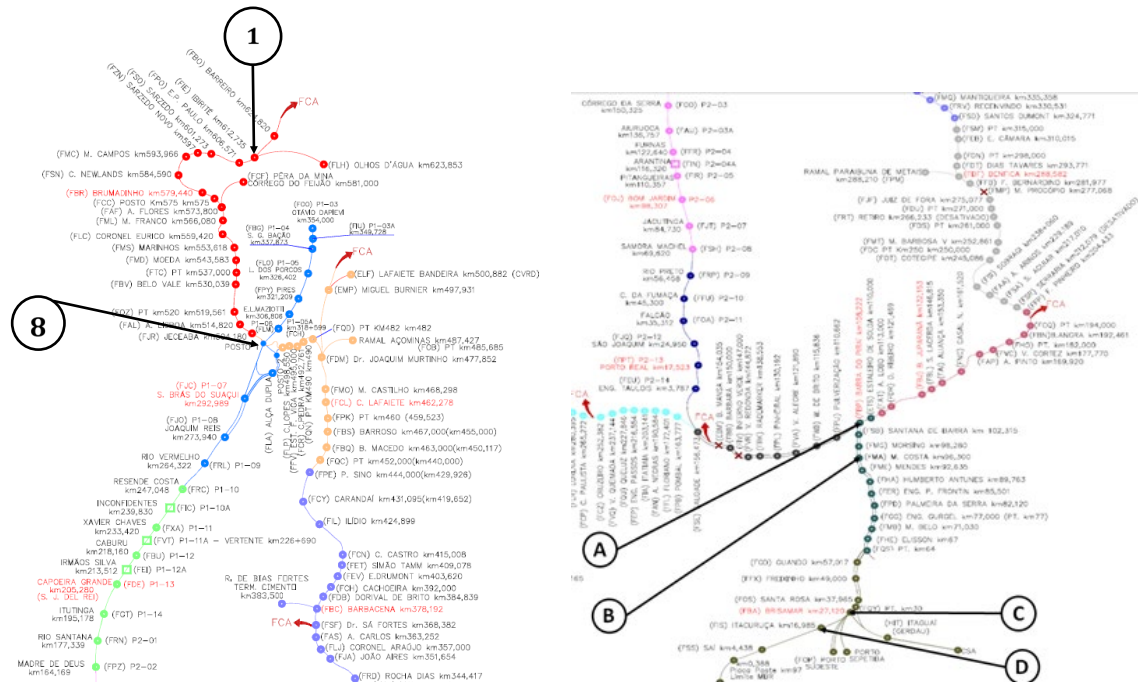


Figure 15. Track sections for data acquisition and analysis.

Table 2. Track segments and inspection dates.

Track Segment	Date 1	Date 2	Date 3	Date 4	Date 5
A-B	07/25/17	10/10/17	02/22/18	02/28/18	07/17/18
B-C	08/03/17	09/04/17	10/24/17	11/17/2017	
1-8	08/01/17	09/13/17			

For this study, the longest inspection file for each segment was selected from the available inspection dates (highlighted cells in Table 2). This represented approximately 44, 7, and 100 miles for A-B, B-C, and 1-8, respectively.

EXPLORATORY DATA ANALYSIS

In order to understand the variation in typical Yrel values, density distributions were created for the three study routes for the left and right rails independently and are shown in Figure 16.

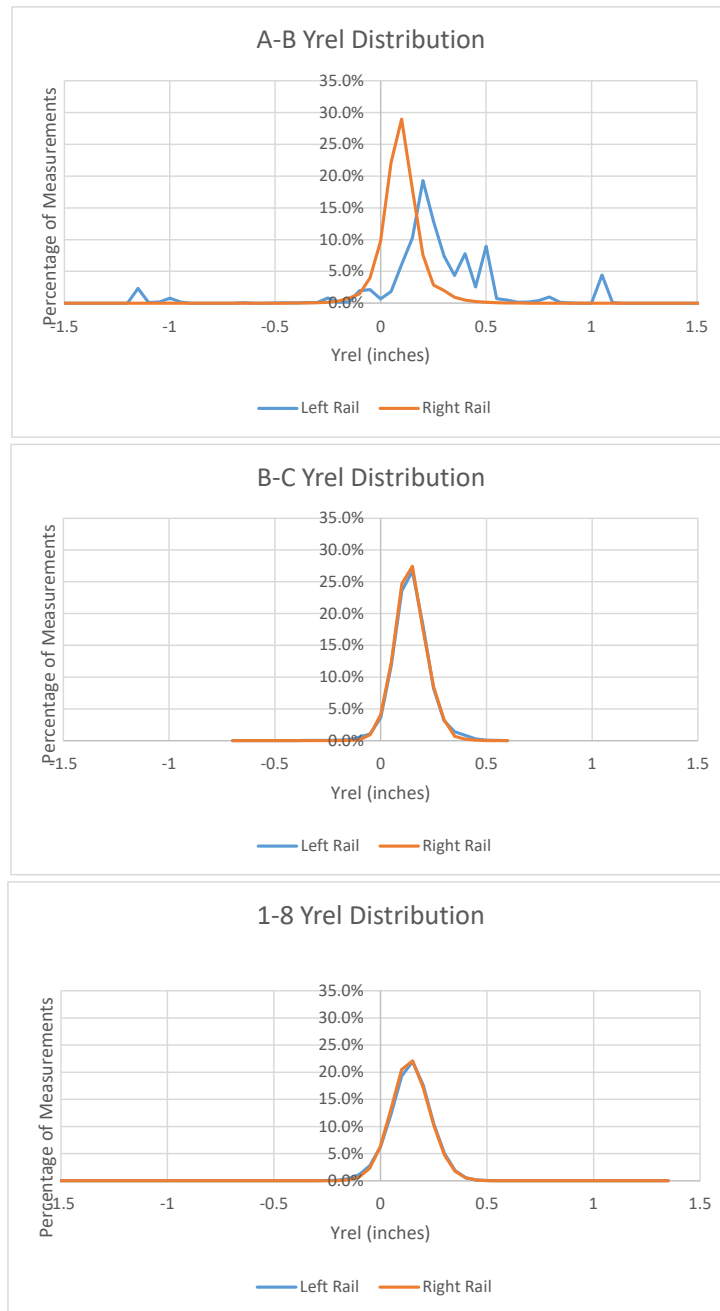


Figure 16. Density distributions for the three study routes.

Figure 16 clearly shows that, in general, the three segments behave quite differently. Segment 1-8 has a wider distribution and Segment B-C has a narrower distribution, indicating a somewhat more uniform track stiffness, and both rails show identical behavior. Segment A-B, however, shows two distinct distributions for the left and right rails (with a shift in mean, and more variation), as well

as several significant extreme measurements (outliers). The left rail sensor was confirmed to have reliability issues on this day of inspection. Summary statistics for these data are shown in Table 3.

Table 3. Yrel summary statistics for the three segments.

	A-B Left Yrel (in)	A-B Right Yrel (in)	B-C Left Yrel (in)	B-C Right Yrel (in)	1-8 Left Yrel (in)	1-8 Right Yrel (in)
Minimum	-2.03	-0.52	-0.64	-0.19	-1.51	-0.31
Maximum	2.53	1.07	0.56	0.48	1.34	0.55
Average	0.22	0.07	0.12	0.12	0.12	0.12
St. Dev.	0.40	0.09	0.09	0.07	0.10	0.09

Figure 17 shows a comparison of the right rail Yrel distribution for the three study segments, which clearly shows the mean and variation by segment.

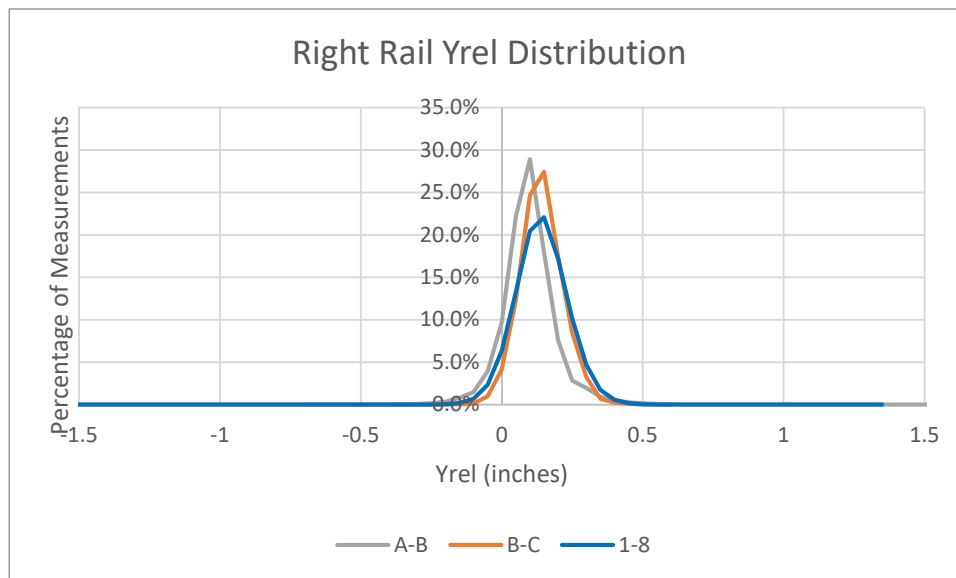
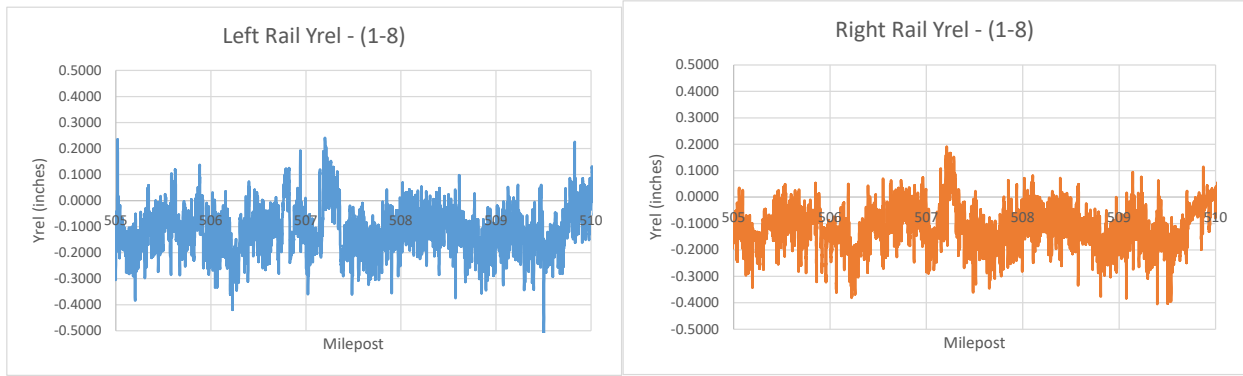
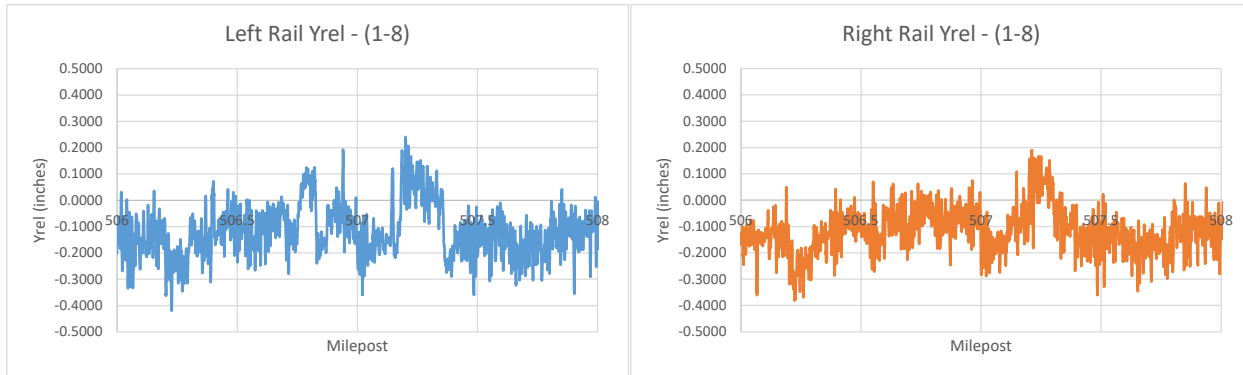


Figure 17. Right rail Yrel distribution comparison.

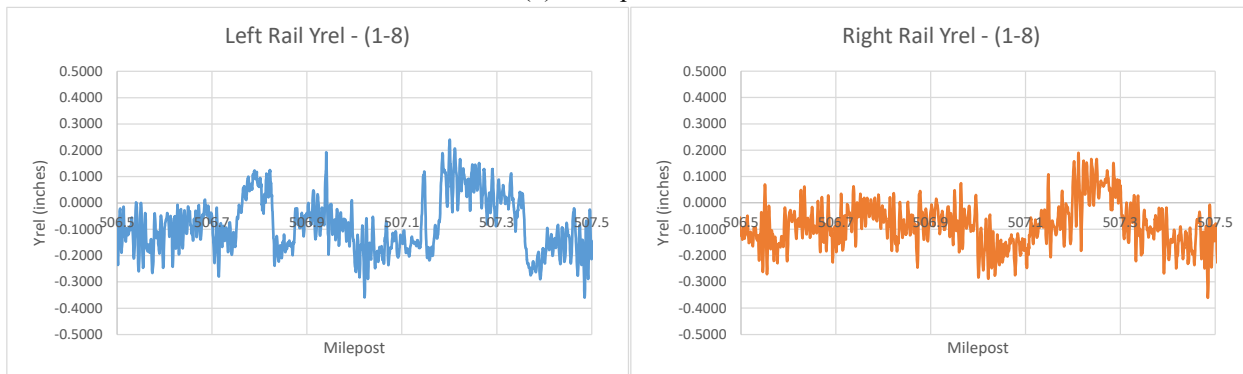
These distributions provide a good indication of the overall stiffness and stiffness variation for the track measured. However, the goal of this study was to evaluate abrupt stiffness changes, particularly at bridge approaches. Typical output of the Yrel data for a 5-mile length of track is shown in Figure 18. This figure (part a) shows the significant variation of Yrel along the track, where the running mean is indicative of the track stiffness. For example, a stretch of stiffer track, bounded by stretches of softer track, can be identified between miles 506 and 508 (see part b). This becomes more obvious in part c.



(a) Milepost 505 to 510



(b) Milepost 506 to 508



(c) Milepost 506.5 to 507.5

Figure 18. Typical Yrel output for 5 miles of track.

Figure 18 also clearly shows the high frequency variation of Yrel obtained during inspection. This is further visible in Figure 19, for a selected portion of track (507.0 to 507.5) with two evident stiff stretches of track, one very short (50 ft) and one fairly long (800 ft). This would be representative of a grade crossing followed by a bridge.

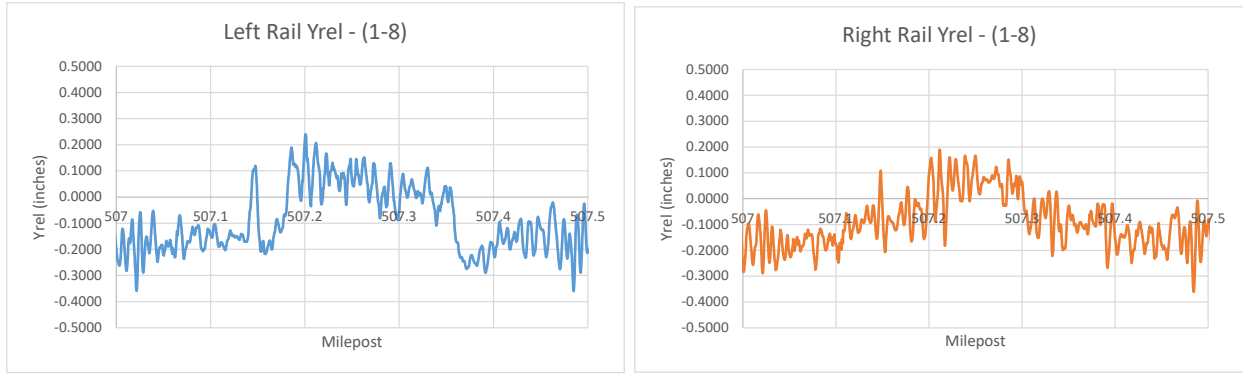


Figure 19. Stiffness variation visible in Yrel (507.0 – 507.5).

A quick frequency analysis of the Yrel data from 507.0 to 507.5 was conducted using a fast Fourier transform (FFT)(see Figure 20) in the R open-source statistical software package (R Core Team, 2019). As expected, the Yrel data result in a low frequency response. In particular, frequencies above 20 Hz were identified as representing the shorter wave Yrel undulations.

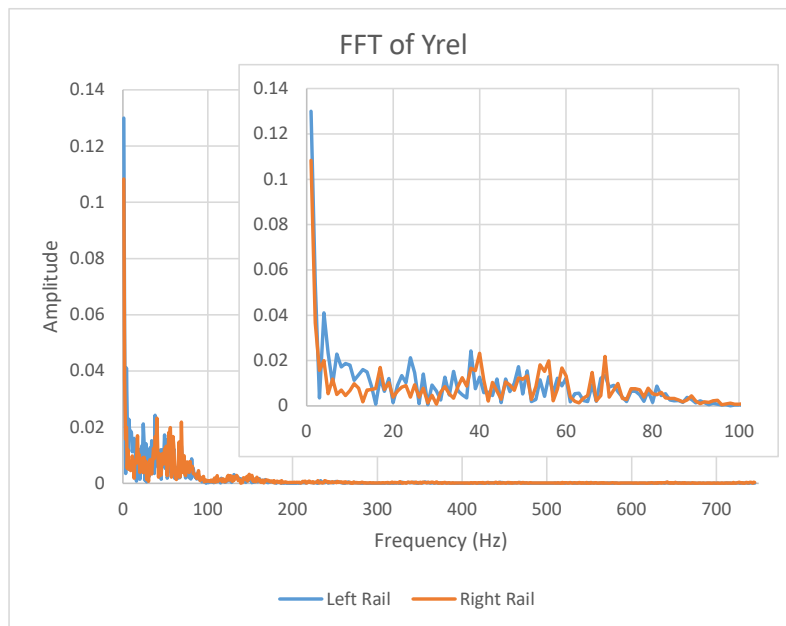


Figure 20. FFT of Yrel data for 507.0 – 507.5

Thus, in order to isolate the effects of abrupt changes in stiffness associated with bridge transitions, some filtering of the data may be required.

DATA PREPARATION

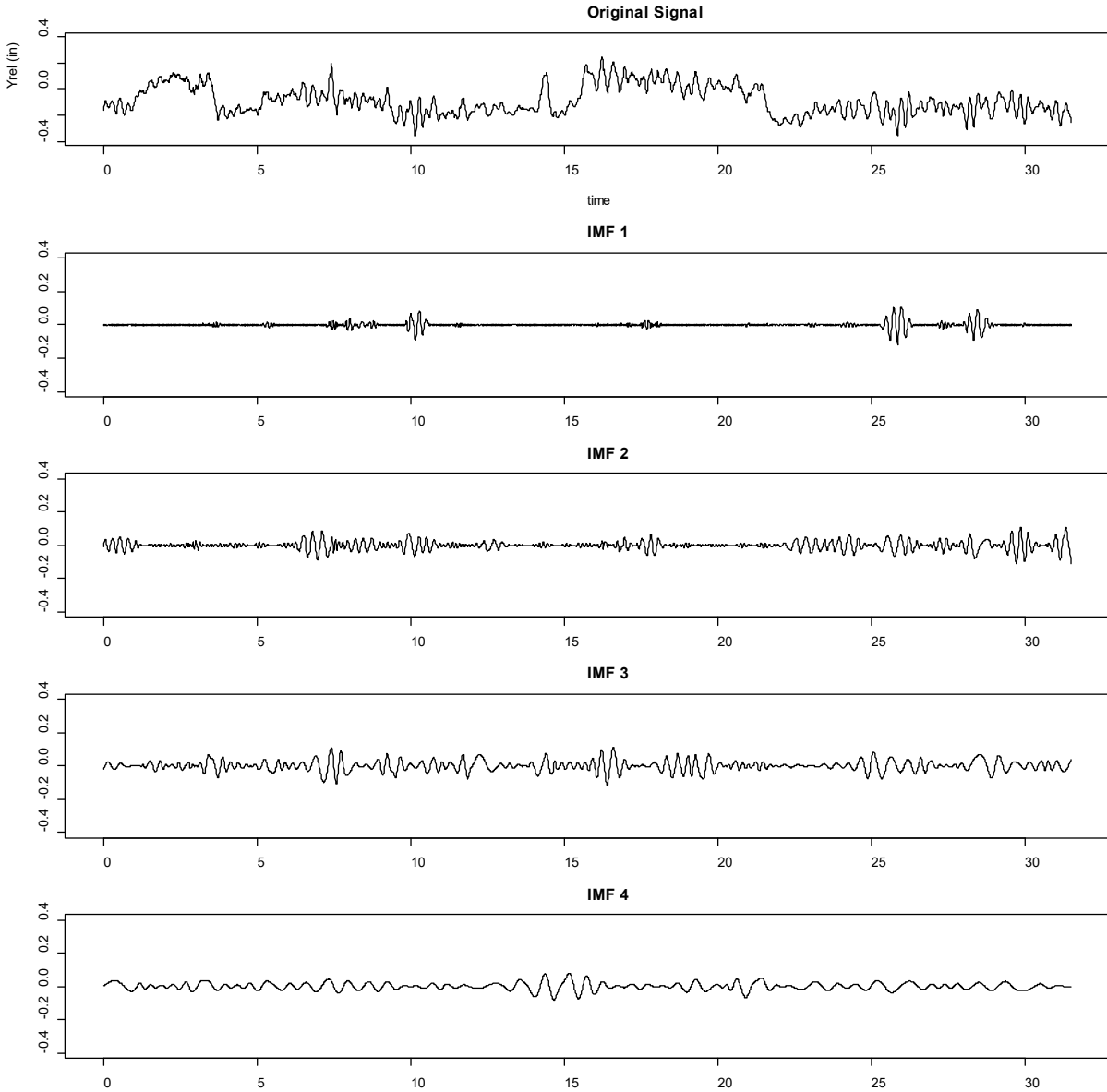
As discussed in the previous section, potential filtering of the Yrel data may be beneficial and is explored further in this section. While FFTs offer a mechanism for filtering data using band pass filtering, the nonstationary multicomponent nature of the data lends itself to empirical mode

decomposition (EMD) (Battista, Knapp, Mcgee, & Goebel, 2007). This can be implemented using the Hilbert Huang Transform (HHT) (Huang et al., 1998).

The intent of the HHT is to separate the original signal into a series of Intrinsic Mode Function (IMF), which when summed will reproduce the original signal. In essence, each of these IMFs (or subset combination) can represent an important component of the signal for analysis.

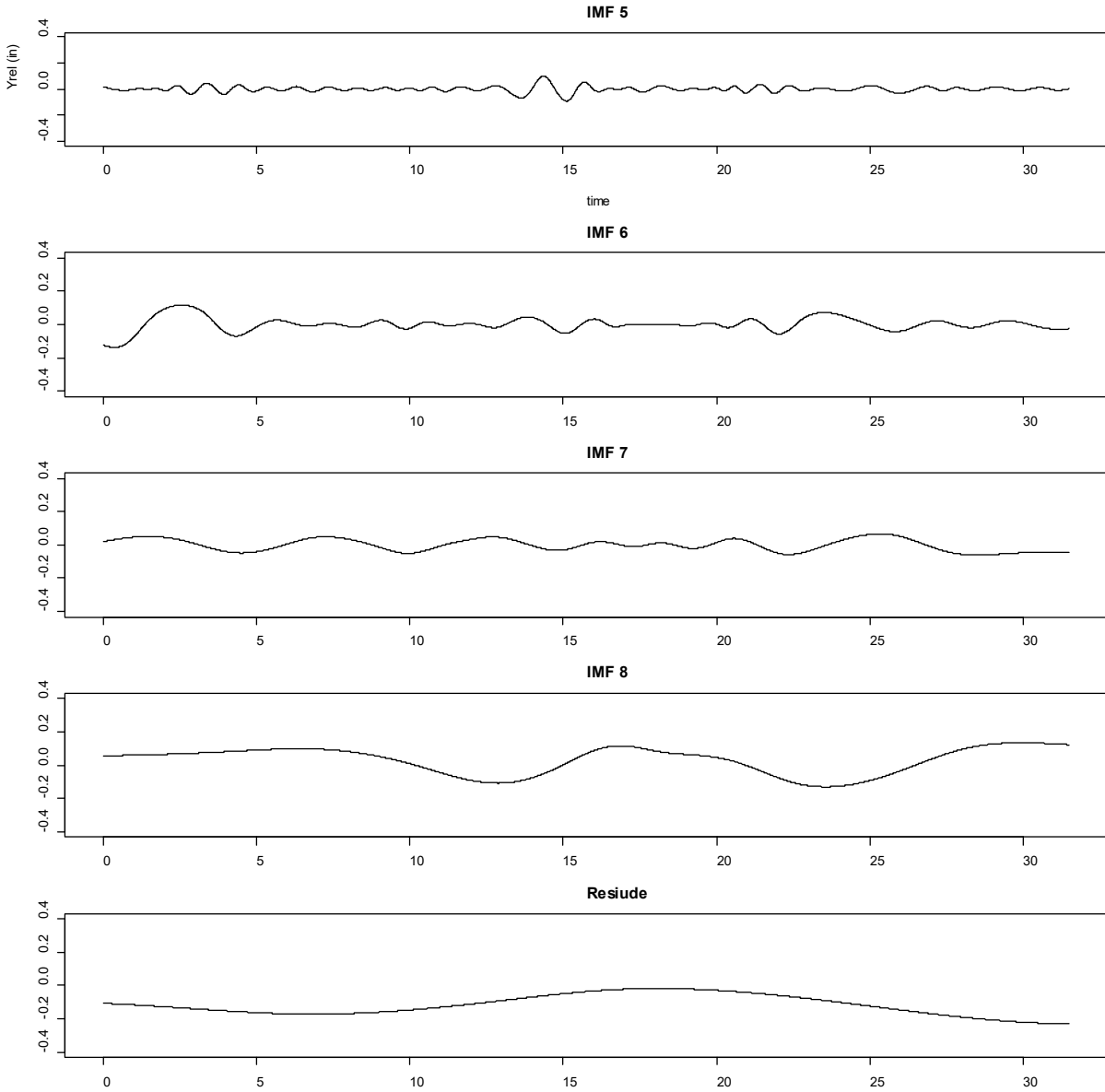
As an example, the Yrel data for the left rail from 507.0 to 507.5 were analyzed using empirical mode decomposition in R. For this analysis, the data were transformed into the time domain, considering a 60-mph vehicle travel speed. The analysis resulted in eight IMFs and a residual signal as shown in Figure 21, along with the original signal. Note that summing IMFs 1–8 and the Residue will result in the original signal.

By inspection, it can be seen that the high-frequency components result in IMFs 1 through 3. Thus, by removing IMFs 1 through 3 from the original signal, the higher-frequency components will be removed, and a smoother signal results. This is shown for comparison in Figure 22, where the black line is the original Yrel and the bolder red line is the smoothed Yrel. This type of smoothing allows for better identification of longer length stiffness variations.



Part (a): Original Signal, IMF 1 to IMF 4

Figure 21. EMD of Yrel (Part a).



Part (b): IMF 5 to IMF 8, and Residue

Figure 22. EMD of Yrel (Part b).

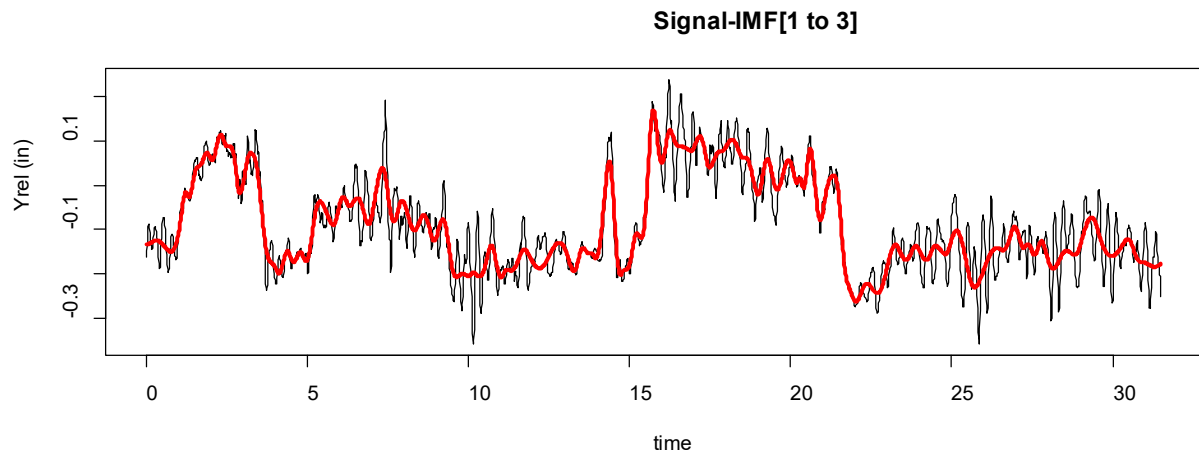


Figure 23. Original and smoothed Yrel.

4. Development of Risk Framework

With the underlying goal of establishing a risk parameter for stiffness transitions, particularly at bridge approaches, it is reasonable to develop a vertical dynamic load-related index. Previous research has shown that a passing vehicle when traversing an abrupt change in vertical stiffness experiences a dynamic “bump” in the track. The effect of this “bump” is a function of the axle load, speed of the traveling vehicle, stiffness variation, and track damping, as well as any track irregularities in the running surface (track geometry degradation) of the track due to differential settlement (Zakeri & Ghorbani, 2011). These are the primary factors that lead to increased dynamic load at the transition of parent track and bridges. These effects lead to increased maintenance requirements in the form of shortened tamping cycles (Milosavljevi, Popovi, & Lazarevi, 2012; Sasaoka & Davis, 2005), and one study developed a model for predicting the rate of settlement (Davis & Chrismer, 2007).

Several researcher have looked at the forces generated due to the “bump” associated with stiffness transitions (Kang et al., 2006; Liang, Ghazel, Cazier, & El-Koursi, 2018; Palese et al., 1998; Wang, Silvast, Markine, & Wiljanen, 2017) and one study instrumented several bridge approaches to quantify differential deflection over the “bump” (Mishra, Tutumluer, & Stark, 2012).

DYNAMIC SIMULATION

In order to understand the dynamic vertical load associated with stiffness transitions, the model developed in Simulink and previously presented can be applied to the Yrel data. Unlike a uniform step change in deflection at the stiffness transition (see Figure 6) due to an idealized and uniform track support, the stiffness varies around a mean value and is related to the deflection, or Yrel data (see Figure 22). The actual Yrel data can in turn be used as a forced input to the dynamic simulation model. Recall that the model requires a vertical velocity input (V_y). This can be achieved by differentiating the Yrel data with respect to time for a defined vehicle speed (V) using central difference numerical differentiation, as follows:

$$V_y(t_i) \cong \frac{Yrel_{i+1} - Yrel_{i-1}}{2dt}, \quad (i = 2, \dots, N - 1)$$

Where

$$dt = \frac{dx}{V}, \text{ where } dx = 1 \text{ ft for this data}$$

Utilizing the equation above, the resulting vertical velocity profile (vehicle traveling at 60 mph) for the left rail for a half mile of track (MP 507.0 to 507.5) based on the measured Yrel data is

shown in Figure 23. The vertical velocity is shown in the time domain for the raw data and for the data smoothed using the HHT (First three IMFs removed) filtering technique.

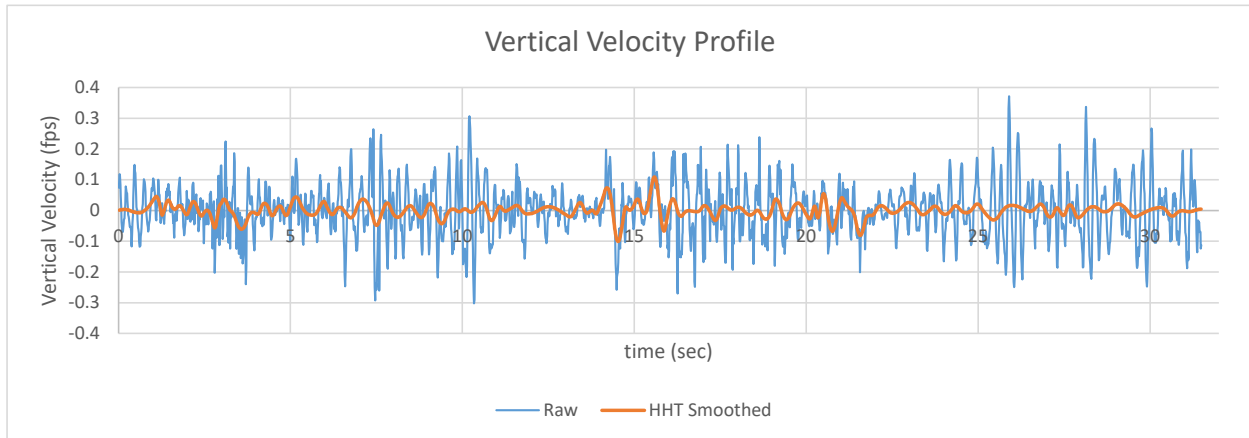


Figure 24. Vertical velocity profile for MP 507.0 to 507.5.

Note that, while the HHT filtering algorithm clearly smoothed the Yrel signal (see Figure 22) to help identify average stiffness, the effect on vertical input velocity is quite drastic. This becomes clear when simulating the velocity profile using the developed Simulink model. The Simulink force outputs are shown in Figure 24, for the raw Yrel data (shown in green) and the HHT smoothed Yrel data, and their corresponding vertical velocity inputs, for a 286,000-lb car and associated stiffness/damping characteristics. This figure shows maximum vertical dynamic impact force increases of the order of 40%.

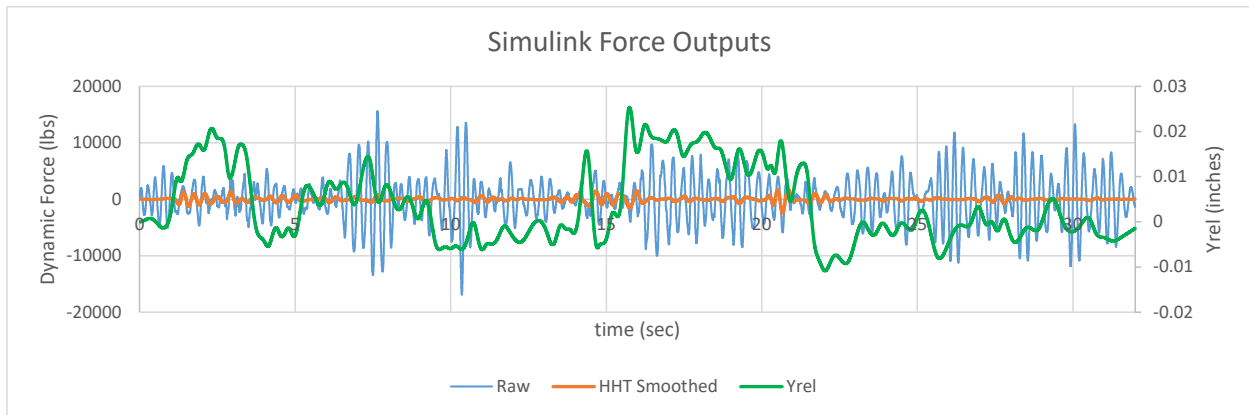


Figure 25. Simulink vertical dynamic force output.

Figure 24 clearly shows that the predicted vertical force is drastically reduced when using the filtered Yrel data. This is not surprising considering the reduced velocity input. However, the smoothed output does show variation in the transition zone.

In addition, and most important, the vertical dynamic force component is heavily influenced by rapid, local changes in Yrel. Again, this is not surprising since the Yrel data are influence by the

local track geometry as well as the local stiffness variations. In some cases, these local variations result in higher impact forces than those caused by the stiffness variations. This has been noted by others (Plotkin, Davis, Gurule, & Chrismer, 2006), where simulation and field testing on high-speed track showed a 10% increase in dynamic force associated with only the stiffness transition considered.

SPEED EFFECT

One of the important parameters that affect the dynamic impact at a stiffness transition is the speed of travel of the vehicle. To better understand this, the BOEF step change in stiffness (see Figure 6) was investigated in more detail. The associated deflection map was converted to a vertical velocity input for the simulation model for speeds of 40 to 80 mph in 10 mph increments, as shown in Figure 25. Note the change in peak velocity and time of duration of the velocity input.

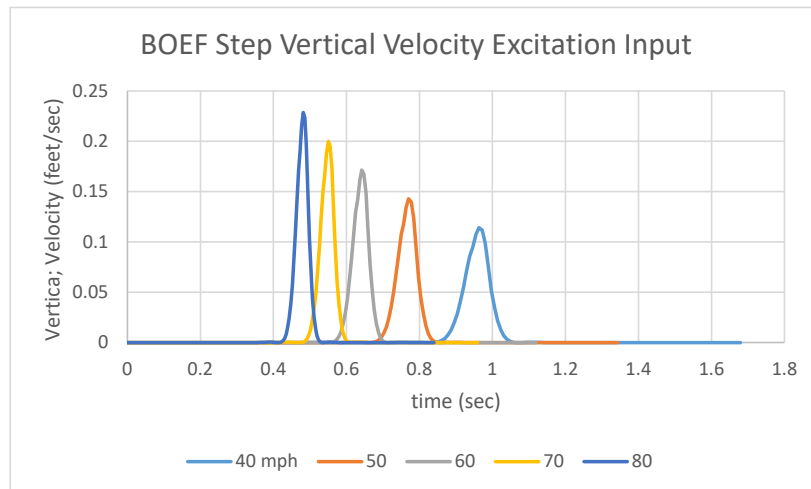


Figure 26. Velocity excitation for BOEF step change in stiffness for various speeds.

Each of these velocity input profiles was simulated using the Simulink model. The results of these simulations are shown in Figure 26. Note the increase in downward force (positive), followed by a relaxation (negative), and a damped oscillating response. The peak force increases with increased speed as expected.

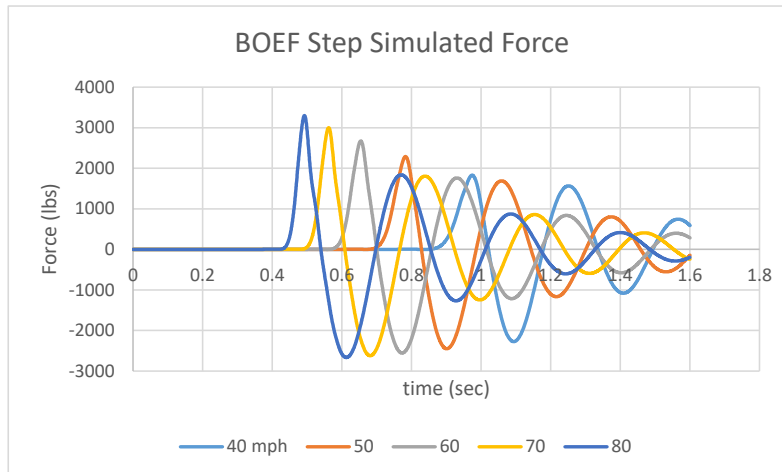


Figure 27. Simulated dynamic force output for various speeds.

The primary outputs were summarized for the speed analysis and are shown in Table 4. This table shows the speed of analysis and vertical velocity input, as well as the peak dynamic force (downward) and impact factor ($1 + F_{dynamic}/F_{static}$). In addition, a comparable analysis was conducted using the simplified slope method previously presented for the driving slope of the BOEF deflection map.

Table 4. Summary output for speed sensitivity.

V (mph)	dy/dt (fps)	Simulation Dynamic Force (lb)	Simulation Impact Factor	Slope Method Dynamic Force (lb)	Slope Method Impact Factor
40	0.1143	1,828.2	10.5	2,374.0	1.07
50	0.1429	2,288.2	1.06	2,967.5	1.08
60	0.1714	2,671.2	1.07	3,561.0	1.10
70	0.2000	3,001.3	1.08	4,154.5	1.12
80	0.2286	3,299.5	1.09	4,748.0	1.13

The results presented in Table 4 were plotted and are shown in Figure 27. As can be seen from this figure, the vertical velocity input changes linearly with speed, as expected. In addition, as expected for the equation for the simplified slope method, the force increases linearly with an increase in vehicle speed. The peak forces from the Simulink simulation model appear to increase with an increase in speed according to a second-order polynomial (consistent with work done by Spiroiu & Crciun (2016)) but are very nearly linear for the purposes of this analysis. As previously shown, for the ideal case analyzed here, the slope method predicts forces up to 40% higher than the dynamic simulation model.

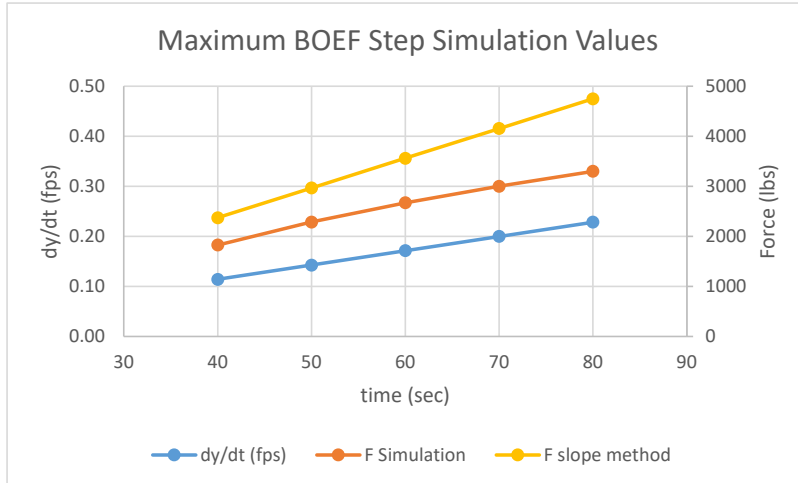


Figure 28. Summary plot of speed sensitivity results.

IDENTIFICATION OF STIFFNESS TRANSITION ZONES

In order to isolate transition zone areas without external input², a simplistic algorithm was developed to identify these locations. This, in turn, allows for isolating impact forces at transition zones for comparative purposes, while excluding local impact forces. The approach used was to evaluate two parameters directly from the *Yrel* data: stiffness differential ($\Delta Yrel$) within a window, and the square of the Pearson product moment correlation coefficient (R^2) of a line fit through the window. This is defined by the following two equations:

$$\Delta Yrel_i = ABS(Yrel_{i+\Delta x/2} - Yrel_{i-\Delta x/2})$$

Δx = length of window in feet-1 (number of consecutive measurement points)

$$R^2_i = \frac{[\sum(x_i - \bar{x})(y_i - \bar{y})]^2}{\sum(x_i - \bar{x})^2 \sum(y_i - \bar{y})^2}$$

In essence, if a window of *Yrel* points of defined length (Δx) has an absolute change in elevation of defined height ($\Delta Yrel > \Delta Yrel_{lim}$), and the slope of a line fit through the measurement points has a good fit ($R^2 > R^2_{lim}$), a point in a transition zone is defined. The entire zone is then defined as the bounding points within the zone $\pm \Delta x / 2$.

Considering a window length of 23' ($\Delta x / 2 = 11$), $\Delta Yrel_{lim} > 0.2''$, and $R^2_{lim} > 0.8$, Figure 25 shows the defined transition zones for MP 507.0 to 507.5. This algorithm can be refined using alternate

² This requires an additional data source of known bridges. While this is commonly known for larger railroads (usually by milepost and GPS coordinates), these data were not available for this study.

limit values, or more sophisticated processes, but for the purposes of this study, this simplistic method for identifying transition zones is suitable.

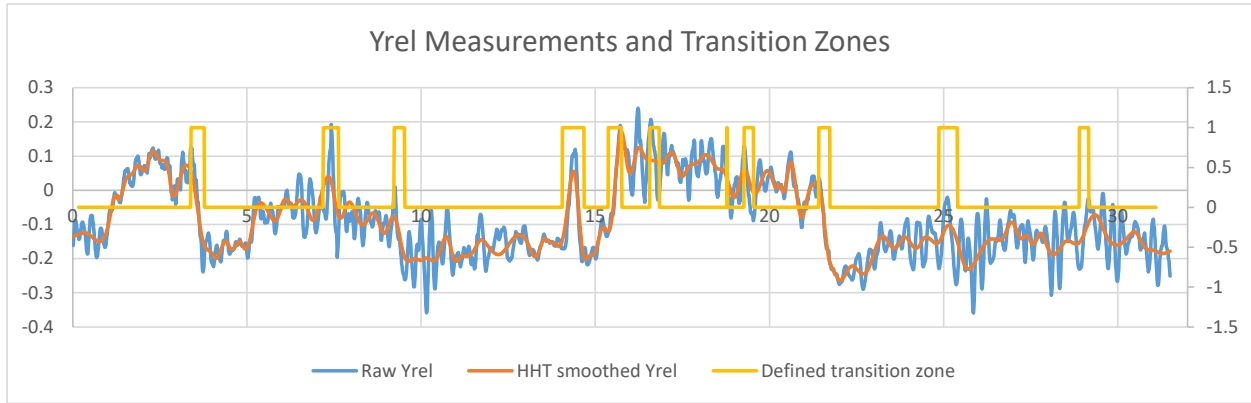


Figure 29. Defined transition zones.

TRANSITION RISK MODEL

Considering all of the above, a risk index can be created for each measurement of *Yrel*. The risk index is in the form of a dynamic load impact factor as follows:

$$RISK_i = TZ_i * (1 + Pd_i/Pst)$$

Where

$$TZ_i = \begin{cases} 1, & \text{for a defined transition zone} \\ 0, & \text{for everywhere else} \end{cases}$$

$$Pd_i = \begin{cases} Pd \text{ from Simulink} \\ \text{or} \\ \frac{(Yrel_{i+1} - Yrel_{i-1})}{x_{i+1} - x_{i-1}} V\sqrt{km} \end{cases}$$

Pst = static wheel load

In the above, the dynamic force augment can be determined from simulation modeling, such as the Simulink model developed herein, or some other more sophisticated simulation model. This is often impractical for large amounts of data. Alternatively, the slope method can be implemented both practically and easily, as defined in the above equation. A comparison is shown in Figure 29.

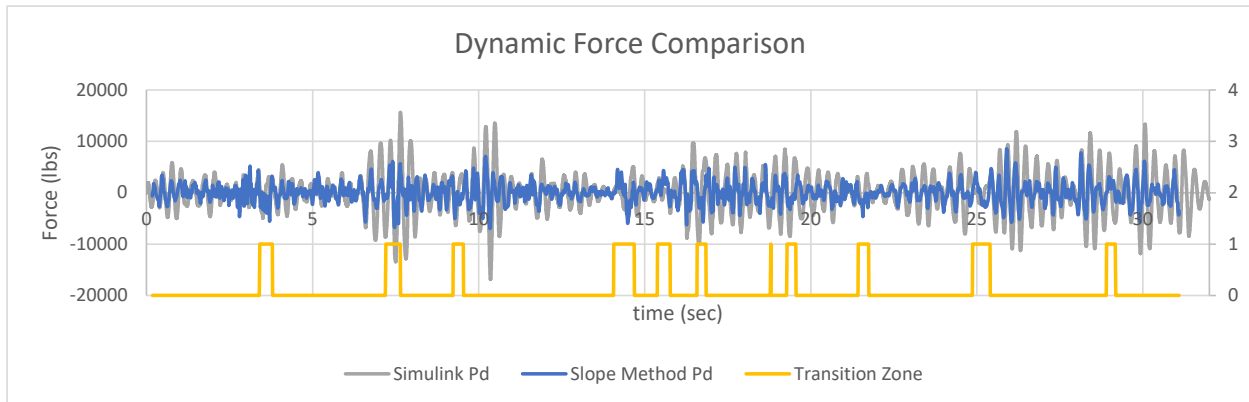


Figure 30. Comparison of Simulink and slope method.

When considering actual data, it appears that for the example shown, the slope method slightly understates the forces predicted by the Simulink model. This is particularly true in the localized location of rapid change of Y_{rel} . Figure 30 shows an example for several transition zones.

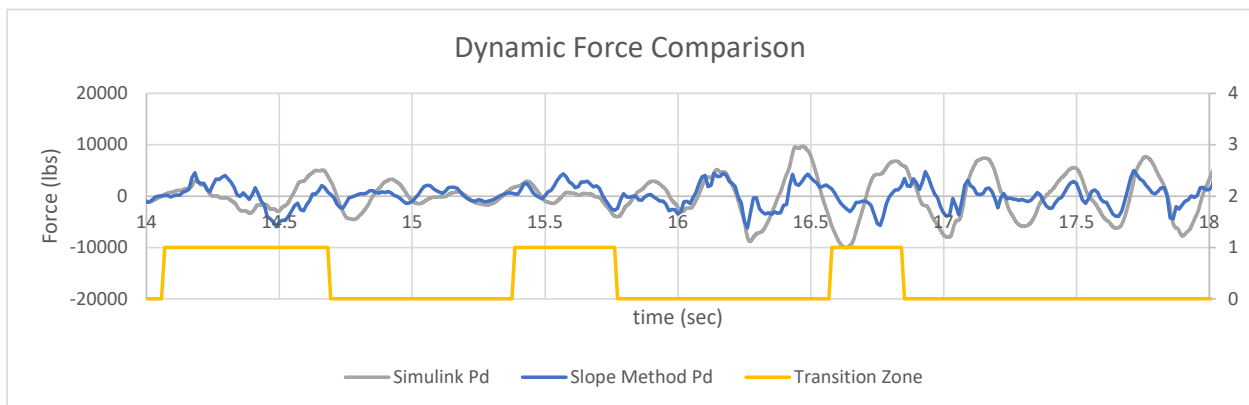


Figure 31. Transition Zone comparison of Simulink and slope method.

Considering representative values for dY_{rel}/dx , a sensitivity analysis on impact factor was performed for the 286,000-lb car for several speeds, as shown in Figure 31. This figure shows that the slope method can result in risk factor (dynamic impact factors) of greater than 1.25 for steep slopes (large dY_{rel}/dx) and high speeds can result.

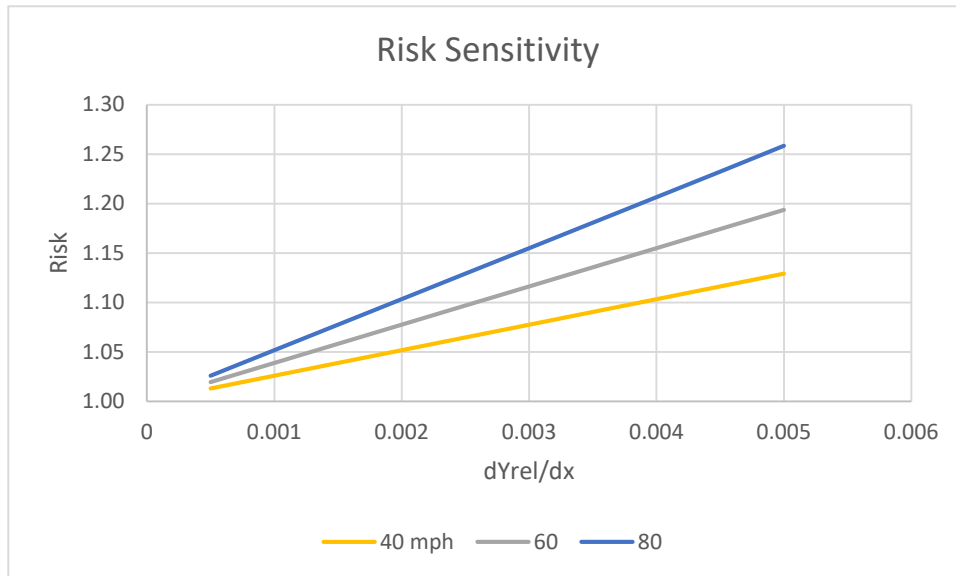


Figure 32. Sensitivity analysis of risk model.

5. Application of Risk Framework

An application of the transition zone risk model presented in the previous section was performed for the three study segments, utilizing the slope method equation. This approach was used based on its ease of implementation and ability to be incorporated in real time on the inspection vehicle.

Figure 32 shows an example of the application of the risk framework for milepost 507.0 to 507.5. The top plot shows the left rail Y_{rel} values (in units of feet) as well as the identified transition zones. The bottom plot shows the calculated risk values (impact factor) within the transition zone, along with the maximum/peak value within the zone³. Note that the risk value within the zone traverses around 1.0. This is due to the dynamic force interaction within the zone and the maximum, or peak, value is of interest.



Figure 33. Example application of risk framework.

³ The maximum value is the yellow square and is shown at the end of the zone and is considering the maximum risk value for the entire zone.

This same approach was applied for the entire length of track in each of the three study segments. Thus, for more than 100 miles of track, the transition zones were identified and the maximum risk factor calculated for each transition zone. Table 5 contains a summary for each of the three study segments. The left portion of the table provides summary statistics for the risk value for every point within the transition zone total length. Of particular interest is the right portion of the table, where each transition zone was analyzed to determine the maximum risk value within the transition zone itself, as discussed in Figure 32. For example, Zone 1-8 had 1,361 transition zones on the left rail that ranged in length from 23' to 163' with an average value of 30.9'. The corresponding risk indices ranged from 1 to 1.86 with an average of 1.12. A transition zone is defined for the track, not the rail side; however, the data were analyzed per rail. In addition, since the location of bridge approaches was not known, other stiffness transition locations (culvert, grade crossing, changes in subgrade, etc.) were identified.

Table 5. Summary statistics of risk values for each study.

	Within Zone Statistics						Zone Maximum Statistics					
	Left Rail			Right Rail			Left Rail			Right Rail		
		Meas	Risk		Risk	Number of Zones	Length (ft)	Risk	Length (ft)	Risk		
Zone AB						482			1390			
Total Number	232525	Minimum	-3.69		0.16	Minimum	23	1	23	1		
Number in TZ	16604	Maximum	5.51	60503	1.83	Maximum	226	5.51	417	1.83		
Percent in TZ	7.1%	Average	1.00	26.0%	1.00	Average	34.4	1.28	43.5	1.16		
		Std Dev	0.05		0.06	Std Dev	2.1	0.06	4.7	0.09		
Zone BC						108			84			
Total Number	21948	Minimum	0.59		0.74	Minimum	23	1	23	1		
Number in TZ	3408	Maximum	1.45	2737	1.32	Maximum	85	1.45	103	1.32		
Percent in TZ	15.5%	Average	1.00	12.5%	1.00	Average	31.6	1.14	32.6	1.11		
		Std Dev	0.04		0.03	Std Dev	2.5	0.08	2.3	0.07		
Zone (1-8)						1361			1494			
Total Number	325177	Minimum	-0.05		0.60	Minimum	23	1	23	1		
Number in TZ	42053	Maximum	1.86	47714	1.42	Maximum	163	1.86	149	1.42		
Percent in TZ	12.9%	Average	1.00	14.7%	1.00	Average	30.9	1.12	31.9	1.12		
		Std Dev	0.03		0.04	Std Dev	2.3	0.07	2.6	0.08		

In order to understand the distribution of resulting risk values, Figure 33 shows the probability density function and cumulative density function for each rail, with separate plots for each of the study segments. This figure shows the mean and variation of the risk factors, allowing for classification of a transition with respect to risk associated with dynamic impact. The average risk in the transition zone area ranges from 1.11 to 1.16, excluding the left rail in Zone AB (1.28), which was shown to have issues with the measurement data.

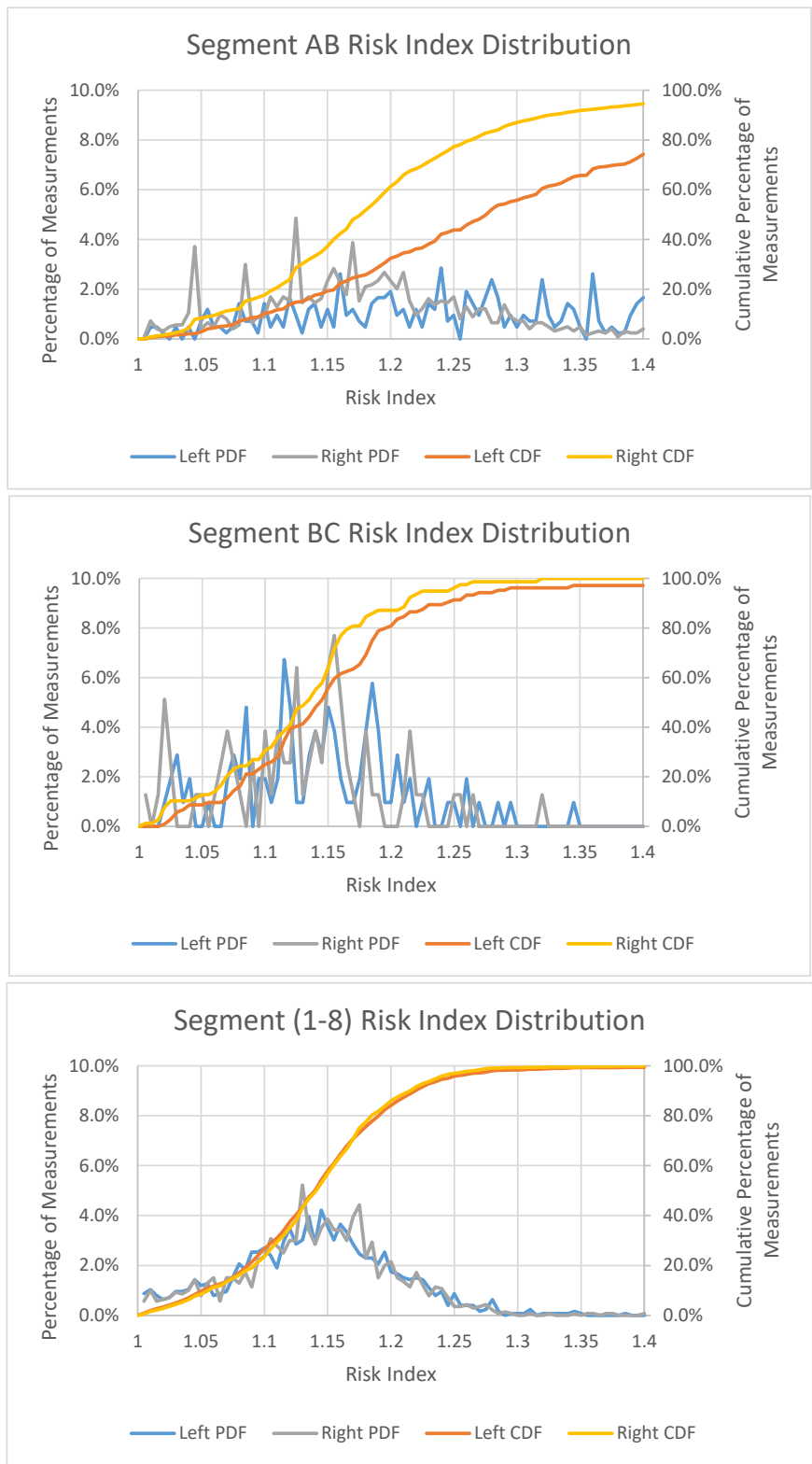


Figure 34. Max risk distribution for each study segment.

Given the distribution, it is reasonable to set thresholds for classifying the transitions. The average range of risk was shown to be 1.11 to 1.16 (which is a dynamic impact factor), which is consistent with report values of > 1.1 from previous studies (Plotkin et al., 2006). Thus, for exemplary purposes, the following thresholds⁴ were set, as shown in Table 6.

Table 6. Example risk thresholds.

	Classification	Range
< 1.1	Low Risk	No action required. Behaving reasonably.
1.1–1.25	Moderate Risk	Potential for moderately accelerated degradation. Monitor.
1.25-1.4	High Risk	High risk if accelerated degradation. Candidate for further analysis.
> 1.4	Very High Risk	Candidate for remedial action such as subgrade remediation, addition of transition material, matched pads technique, etc.

Note that the above thresholds represent varying classes of maintenance and remediation requirements and do not correlate to safety due to the low level of dynamic loading. Applying these thresholds to the risk values calculated for the three study segments results in Table 7.

Table 7. Application of thresholds summary.

	Segment AB				Segment BC				Segment (1-8)			
	Left Rail		Right Rail		Left Rail		Right Rail		Left Rail		Right Rail	
	Num	Pct	Num	Pct	Num	Pct	Num	Pct	Num	Pct	Num	Pct
< 1.1	43	10.2%	218	17.6%	26	25.0%	24	30.8%	336	26.7%	330	23.6%
1.1 - 1.25	141	33.6%	748	60.5%	69	66.3%	52	66.7%	876	69.6%	1031	73.7%
1.25 - 1.4	128	30.5%	204	16.5%	6	5.8%	2	2.6%	40	3.2%	36	2.6%
> 1.4	108	25.7%	67	5.4%	3	2.9%	0	0.0%	7	0.6%	1	0.1%
	420		1237		104		78		1259		1398	

Table 7 allows for quickly identifying the number of transition zones that fall into a given category. Note that Segment AB has a much larger proportion of segments in the poorer categories (higher risk factor). This is most likely due to the measurement equipment issues reported. In addition, the data allow for determining the total length of transitions in various maintenance categories for defining maintenance requirements.

⁴ Note that these thresholds are representative and further research is required to establish appropriate thresholds.

6. Concluding Remarks

Research has shown that abrupt vertical track stiffness variations at bridge abutments can cause accelerated track geometry degradation, resulting in significantly increased maintenance costs in these locations. While some researchers estimated significantly increased vertical dynamic forces in these areas, others showed that a 10% increase can be realized.

SUMMARY OF RESEARCH

The research conducted herein was aimed at utilizing readily available track measurement data, specifically vertical track deflection data (MRail), to develop a risk index for stiffness transitions. A dynamic simulation approach was utilized to develop the risk index. It was shown that dynamic simulation modeling is an effective means for developing a dynamic impact factor at stiffness transitions, due to the abrupt change in vertical elevation as a vehicle runs over the transition zone. While commercially available sophisticated simulation models provide multiple degrees of freedom to develop force and motions of multiple car components, the force at the track is of predominant interest. These models are complicated to implement and are computationally intensive. For the purposes of this study a simplified dynamic simulation approach can be used.

Two approaches were studied: an eighth-car freight model developed in Matlab/Simulink that responds to a vertical velocity forced input, and a simplified single-sprung mass with a vertical velocity impulse based on the slope of travel of the mass. The vertical velocity forced input can be developed directly from the MRail vertical track deflection measurement data and the vehicle speed. This vertical velocity input can be input to the dynamic simulation model (either method described above) and the dynamic force and corresponding dynamic impact factor calculated, which defines the risk index.

Thus, a risk index can be determined based on the following:

- Weight of the vehicle
- Speed of the vehicle
- Suspension characteristics
- Vertical stiffness transition (from MRail data)

This risk index was then applied to three study segments. For this application, locations of bridges were not explicitly defined. Railways generally have a database of these locations. Since they were not readily available, a simplistic algorithm for identifying stiffness transition zones was

developed. The results of the application showed that quite a number of stiffness transitions were identified, considerably more than the estimated number of bridges. This is to be expected as grade crossings, culverts, and other track structures will result in vertical track deflection data (MRail) that exhibit transition zone response. In addition, naturally occurring transition zones due to significant change in subgrade characteristics will result. These transition zones varied in overall length.

The risk index was then calculated for each of these zones, both the change in force throughout the zone as well as the maximum value within the zone. In order to understand the relative distribution of the resulting index values, probability density plots were developed. Based on these plots, as well as results of other researchers, a series of potential thresholds for the risk index were introduced and the transition zones classified based on these thresholds. This type of analysis allows the railroad to classify its track and develop maintenance and remediation plans for transition zones.

Implementation of this risk model, in the manner conducted herein, can be done in real time on the inspection car due to its practical nature and straightforward calculation technique, or alternatively offline using an eighth freight car model, as developed herein.

FUTURE RESEARCH

There are several other factors that can augment the risk over and above the dynamic impact factor approach. The implementation was for maximum speed for one heavy-axle-load car type. The model could easily be applied for different car types and travel speeds, based on the type of traffic and track speed limits.

In addition, the type of traffic can influence the allowable dynamic impact forces. This can be handled using a matrix of thresholds (different thresholds for different types of traffic), or augmenting the index based on type of traffic (passenger, hazardous materials, etc.).

The density of trains, along with the axle load and speed of travel, will have a direct effect on the risk of accelerated degradation and failure. Track settlement at a bridge abutment will be affected by the stiffness transition as well as local geometry imperfections and happens over many load cycles. It was shown that an increase in vertical load (associated with a stiffness transition) will result in a change in differential settlement of approximately 75% of the change in load (Plotkin et al., 2006). This differential settlement manifests itself in track geometry deformations, for which railroads have strict safety criteria. The risk index can be augmented to incorporate traffic density (millions of gross tons, MGT) and track settlement algorithms. The data collected for this research were only for a one-year time frame and did not provide enough differentiation over time to make a data-driven analysis possible.

References

- Battista, B. M., Knapp, C. C., Mcgee, T., & Goebel, V. (2007). Application of the Empirical Mode Decomposition and Hilbert-Huang Transform to Seismic Reflection Data. *Geophysics*, 72(2):H29–H37.
- Davis, D. D., & Chrismer, S. M. (2007). Track Differential Settlement Model. *Proceedings of the 2007 ASME/IEEE Joint Rail Conference*, 1–5.
- Farritor, S., and Fateh, M. (2013). *Measurement of Vertical Track Deflection for a Moving Rail Car*. Federal Railroad Administration, Report No. DOT/FRA/ORD-13/08, Washington, D.C.
- Hetényi, M. (1946). *Beams on Elastic Foundation: Theory with Applications in the Fields of Civil and Mechanical Engineering*. Michigan: University of Michigan Press.
- Huang, N. E., Shen, Z., Long, S. R., Wu, M. C., Shih, H. H., Zheng, Q., Yen, N.-C., Tung, C. C., and Liu, H. H. (1998). The empirical mode decomposition and the Hilbert spectrum for nonlinear and non-stationary time series analysis. *Proceedings of the Royal Society of London A*, 454(1971):903–995.
- Kang, Y., Yang, S., Lee, H., Kim, Y., Jang, S., & Kim, E. (2006). *A Study of Track and Train Dynamic Behavior of Transition Zone Between Concrete Slab Track and Ballasted Track*. Corpus ID: 22200137, Korea Railroad Research Institute, Uiwang, South Korea.
- Kerr, A.D., & Moroney, B. E. (1993). Track transition problems and remedies. *Bulletin 742*, American Railway Engineering Association, Landover, Maryland, pp. 267–298.
- Kerr, A. D. (2003). *Fundamentals of Railway Track Engineering*. Omaha, NE: Simonas-Boardman Books, Inc.
- Li, D., Otter, D., & Carr, G. (2010). Railway bridge approaches under heavy axle load traffic: Problems, causes, and remedies. *Proceedings of the Institution of Mechanical Engineers, Part F: Journal of Rail and Rapid Transit*, 224:383–390.
- Liang, C., Ghazel, M., Cazier, O., & El-Koursi, E. M. (2018). Developing accident prediction model for railway level crossings. *Safety Science*, 101(June 2017):48–59. <https://doi.org/10.1016/j.ssci.2017.08.013>
- Milosavljević, L., Popović, Z., & Lazarević, L. (2012). Track Stiffness and the Vertical Track Geometry Deterioration Modeling. *FACTA UNIVERSITATIS: Mechanical Engineering*, 10(2):157–162.
- Mishra, D., Tutumluer, E., & Stark, T. D. (2012). Investigation of differential movement at railroad bridge approaches through geotechnical instrumentation. *Journal of Zhejiang University - Science A: Applied Physics & Engineering*, 13(November):814–824. <https://doi.org/10.1631/jzus.A12ISGT7>
- Newman, G. R. (2014). A System to Measure Vertical Track Deflection. In *Big Data in Railroad Maintenance Planning*. Newark, DE: University of Delaware.

- Palese, J. W., Zarembski, A. M., & Katz, L. (1998). *Implementation of a Dynamically Stable Rail-Highway Grade Crossing System and Transition* - Draft Report. Cherry Hill, NJ.
- Plotkin, D., Davis, D. D., Gurule, S., & Chrismer, S. M. (2006). Track Transitions and the Effects of Track Stiffness. In *AREMA Annual Conference*, pp. 1–36. Louisville: AREMA.
- R Core Team. (2019). R: A language and environment for statistical computing. Vienna, Austria.: R Foundation for Statistical Computing.
- Sasaoka, B. C. D., & Davis, D. D. (2005). Implementing Track Transition Solutions for Heavy Axle Load Service. In *2005 AREMA Annual Conference*. Chicago, IL: AREMA.
- Spiroiu, M. A., & Crciun, C. I. (2016). Wheel-rail dynamic forces induced by random vertical track irregularities. In *IOP Conference Series: Materials Science and Engineering*, 147(1):012117, IOP Publishing. <https://doi.org/10.1088/1757-899X/147/1/012117>
- Stark, T., Wilk, S., & Rose, J. (2016). Design and Performance of Well-Performing Railway Transitions. *Transportation Research Record: Journal of the Transportation Research Board*, 2545:20–26.
- The Mathworks, I. (2019). *Matlab*. (R2019b ed.). Natick, Massachusetts.
- Wang, H., Silvast, M., Markine, V., & Wiljanen, B. (2017). Analysis of the Dynamic Wheel Loads in Railway Transition Zones Considering the Moisture Condition of the Ballast and Subballast. *Applied Sciences*, 7(12):1208. <https://doi.org/10.3390/app7121208>
- Zakeri, J., & Ghorbani, V. (2011). Investigation on dynamic behavior of railway track in transition zone. *Journal of Mechanical Science and Technology*, 25:287–292 (February 2011). <https://doi.org/10.1007/s12206-010-1202-x>
- Zarembski, A. M., Palese, J. W., & Katz, L. (1999). Implementation of a Dynamic Rail-Highway Grade Crossing Transition. In *Transportation Research Board Annual Meeting*. Washington, D.C.